



HAL
open science

Did the Younger Dryas to Holocene climate transition favour high seismicity rates in the north-western Alps?

Mathilde Banjan, Christian Crouzet, Pierre Sabatier, Jomard Hervé, Manon Bajard, Francois Demory, Anne-Lise Develle, Jean-Philippe Jenny, Erwan Messenger, Bernard Fanget, et al.

► To cite this version:

Mathilde Banjan, Christian Crouzet, Pierre Sabatier, Jomard Hervé, Manon Bajard, et al.. Did the Younger Dryas to Holocene climate transition favour high seismicity rates in the north-western Alps?. *Sedimentology*, 2023, 70 (2), pp.538-568. 10.1111/sed.13050 . hal-04032433

HAL Id: hal-04032433

<https://hal.inrae.fr/hal-04032433v1>

Submitted on 16 Mar 2023


HAL is a multi-disciplinary open access archive for the deposit and dissemination of scientific research documents, whether they are published or not. The documents may come from teaching and research institutions in France or abroad, or from public or private research centers.

L'archive ouverte pluridisciplinaire **HAL**, est destinée au dépôt et à la diffusion de documents scientifiques de niveau recherche, publiés ou non, émanant des établissements d'enseignement et de recherche français ou étrangers, des laboratoires publics ou privés.



Distributed under a Creative Commons Attribution 4.0 International License

Did the Younger Dryas to Holocene climate transition favour high seismicity rates in the north-western Alps?

MATHILDE BANJAN^{*†} , CROUZET CHRISTIAN^{*}, SABATIER PIERRE[‡], JOMARD HERVÉ[†], BAJARD MANON[§], DEMORY FRANCOIS[¶], DEVELLE ANNE-LISE[‡], JENNY JEAN-PHILIPPE^{**}, FANGET BERNARD[‡], MALET EMMANUEL[‡], NATHANIEL FINDLING^{††}, ALAIN PHILIPPE^{‡‡}, DIDIER JULIEN^{§§}, BICHET VINCENT^{§§}, CLAPOT SYLVAIN^{¶¶} and MESSENGER ERWAN[‡]

^{*}Université Savoie Mont Blanc, Université Grenoble Alpes, CNRS, IRD, Université Gustave Eiffel, ISTERre, Le Bourget du lac, France (E-mail: mathilde.banjan@univ-smb.fr)

[†]IRSN - Bureau d'évaluation des risques sismiques pour la sûreté des installations, Fontenay-aux-Roses, France

[‡]Université Savoie Mont Blanc, CNRS, EDYTEM, Le Bourget du lac, France

[§]Department of Geosciences, MetOs, CEED, University of Oslo, Oslo, Norway

[¶]Aix Marseille Université, CNRS, IRD, INRAE, Collège de France, CEREGE, Aix-en-Provence, France

^{**}Université Savoie Mont Blanc, INRAE, CARTELE, Thonon-les-Bains, France

^{††}Univ. Grenoble Alpes, Univ. Savoie Mont Blanc, CNRS, IRD, Université Gustave Eiffel, ISTERre, Grenoble, France

^{‡‡}Sonar Systems Division, iXblue, La Ciotat, France

^{§§}LCE - Laboratoire Chrono-environnement - CNRS - UBFC (UMR 6249), Besançon, France

^{¶¶}50 Impasse Des Dix Quarts, 38570, Tencin, France

Associate Editor – Nathan Sheldon

ABSTRACT

In the French north-western Alps, several lakes of glacial origin, such as Aiguebelette and La Thuile, present some mass-transport deposits within their sedimentary sequences. These event layers can result from lake sediment destabilization eventually triggered by earthquakes. On Lake Aiguebelette, based on sedimentological, geochemical and magnetic analyses, and high-resolution seismic and bathymetric surveys a *ca* 1 m thick event layer was identified in the deepest lake basin and a synchronous *ca* 2 cm thick deposit in the shallow basin. Age-depth models based on radiocarbon ages reveal that both mass-transport deposits in Lake Aiguebelette occurred around the Younger Dryas – Early Holocene climatic transition (i.e. 11 700 cal BP) time range. In Lake La Thuile, located 30 km away, unique mass-transport deposits (translational slide type) were recorded at the same time range in sedimentary records. Additionally, high-resolution seismic profiles previously acquired in Lake Annecy and Lake Bourget support the hypothesis of significant mass-transport deposits occurring at the Younger Dryas – Early Holocene time range. These outcomes on four north-western peri-Alpine and Alpine lakes highlight the regional occurrence of mass-transport deposits in the Younger Dryas – Early Holocene time range. Seismic and rockfall events are discussed as potential sources of these significant and similarly aged mass-transport deposits. Based on this study and a literature review, the authors suggest that mechanisms induced by rapid climate change and glacial retreat, such as crustal rebound and erosional unloading, could favour the triggering of earthquakes and rockfall events. In the case of mass-transport deposits archived in north-western Alpine lakes during this

time period, this study favours the hypothesis of increased seismicity as the primary source driving process involved.

Keywords Earthquake, homogenite, lakes, north-western Alps, turbidite, Younger Dryas – Holocene.

INTRODUCTION

The recurrence intervals of major earthquakes are often longer than those of instrumental and historical seismological records, although they are key to better understanding regional seismicity and related seismic hazards (Stein & Mazzotti, 2007; Calais *et al.*, 2016). In a given area, palaeoseismology may help constrain the timing of surface-rupturing earthquakes of a given seismogenic source (Atwater *et al.*, 2003; McCalpin, 2009), while lacustrine palaeoseismology allows us to focus on the occurrence of regional events over time (Wilhelm *et al.*, 2016; Kremer *et al.*, 2017; Moernaut *et al.*, 2018). Regional palaeoseismology mostly relies on the identification of indirect effects of seismic ground motions, such as mass-transport deposits (MTDs) or soft sediment deformation structures evidenced within sedimentary sequences (Alsop *et al.*, 2016). MTDs are processes including subaqueous landslides and mass flows that result in the deposition of debris flows, mudflows and turbidites. MTDs are usually recognized by internal chaotic or transparent seismic facies (Jenner *et al.*, 2007; Shipp *et al.*, 2011).

The most common sedimentary facies of an MTD is usually a turbidite. It consists of a coarse, fining-upward, basal part overlain by a clay cap. Additionally, a homogeneous silty-clay part (i.e. the homogenite) can occur between the coarse basal part and the clay cap, leading to a turbidite–homogenite (Tu + Hm) facies. Turbidite–homogenite layers can be imaged as seismically transparent facies in high-resolution seismic reflection profiles (Kastens & Cita, 1981; Cita & Rimoldi, 1997; Beck *et al.*, 2007; McHugh *et al.*, 2011; Eriş *et al.*, 2012).

The synchronicity of such sedimentary markers in several lakes is key to inferring a seismic triggering mechanism at a regional scale (Schnellmann *et al.*, 2005). However, to characterize regional palaeoseismicity through sediment archives, the following main challenges remain: (i) the characterization of source processes; (ii) establishing an accurate and robust chronology; (iii) the identification of the imprint of palaeoearthquakes within sediment sequences; (iv) attributing earthquakes to

their respective seismogenic sources; and (v) estimating the magnitude of identified events.

In the Alps in general and in the studied area in particular (north-western Alps – NW Alps), glacier retreat during the Late Glacial gave birth to a number of natural lakes (Fig. 1). These lakes acted as natural recorders of tectonic, environmental and climatic processes affecting the lakes themselves or their catchments (e.g. Beck *et al.*, 1996, 2001; Beck, 2009; Arnaud *et al.*, 2016). Lake sediments can be regarded as continuous archives in which discrete event layers can be recorded, including MTDs related to the occurrence of seismic events. In the study area, multiproxy sediment analyses in sequences from Lake Bourget (France) allowed the identification of an event layer related to a well-known historical seismic event: the 1822 CE earthquake (Chapron *et al.*, 1999; Beck, 2009). This event has been characterized by an epicentral intensity of VII–VIII (MSK-64 macroseismic scale) in the French database of historical seismicity SIS-FRANCE (Jomard *et al.*, 2021), equivalent to $M_w = 5.5 \pm 0.3$ (Manchuel *et al.*, 2018). In addition, the combination of seismic profiles and sediment core analyses in this lake has allowed the identification of a much thicker and older (approximately 9900 cal BP, Arnaud *et al.*, 2012) MTD, which may also have been triggered by an earthquake. However, the potential source of such an earthquake is unknown. This type of seismically induced deposit has been identified at a broader scale in other peri-Alpine and Alpine lakes, for instance, in Switzerland (see Kremer *et al.*, 2020, and references therein).

In addition, studies based on seismically induced event layers have shown that each lake has its own sensitivity to earthquakes that also evolves through time (Wilhelm *et al.*, 2016; Gastineau *et al.*, 2021). Indeed, it has been proven worldwide that constraining major changes in sedimentation rates and geotechnical properties of sediments is mandatory to assess an accurate seismic record of a lake (Van Daele *et al.*, 2015; Wilhelm *et al.*, 2016; Praet *et al.*, 2017; Rapuc *et al.*, 2018; Gastineau *et al.*, 2021). These major changes are usually influenced by climate change (Peizhen *et al.*, 2001; Delmas

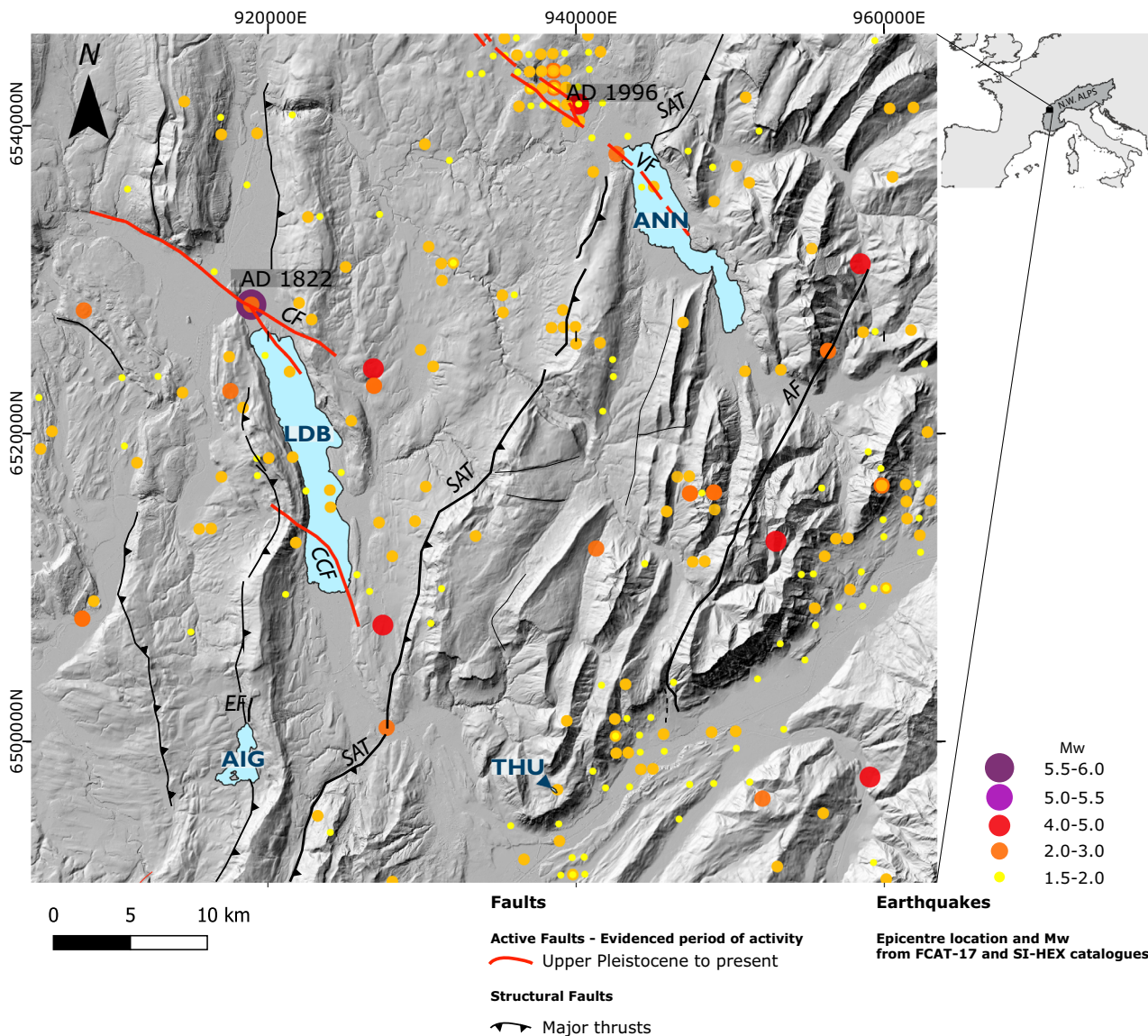


Fig. 1. Seismicity map of the north-western Alps at the border with the French Jura Mountains. Epicentre locations and magnitudes are based on the FCAT-17 and SI-HEX databases (Cara *et al.*, 2015; Manchuel *et al.*, 2018). The main active faults from the Upper Pleistocene are presented in red (CF: Culoz Fault; CCF: Col Du Chat Fault; VF: Vuache Fault). Lakes Aiguebelette (AIG), Annecy (ANN), Bourget (LDB) and La Thuile (THU) are presented in blue in the digital terrain model (IGN RGE ALTI 1 m). Projection: Lambert-93 (EPSG 2154).

et al., 2009). However, human settlement and activities in a watershed may also lead to increased erosion rates and subsequently to higher sedimentation rates within a lake over the Mid to Late-Holocene (Bajard *et al.*, 2016; Rapuc *et al.*, 2018; Gastineau *et al.*, 2021). Therefore, long sediment sequences retrieved in north-western Alpine lakes covering a major climatic transition, such as the Late Glacial to Holocene transition, are expected to have

archived a change in sedimentation rate at this specific time and a subsequent difference in event layer deposition (for example, event layer thickness and frequency) (Wilhelm *et al.*, 2016).

In this paper, two new significant event layers will complete the list of existing MTDs identified in French peri-Alpine lakes and occurring near or at the Younger Dryas – Early Holocene (YD–EH) transition (*ca* 11 700 cal yr BP, Hoek, 2008). These two new event layers were identified

through analyses of two lacustrine records of Lake Aiguebelette and Lake La Thuile (Fig. 1).

Initial focus is on the thickest event layer observed in Lake Aiguebelette, investigated through a multiproxy approach, which constitutes the main analytical contribution of this paper. More specifically, sedimentological, geochemical and magnetic analyses were performed on two sedimentary sequences acquired within the two main basins of the lake, along with radiocarbon dating. To complete these sets of analyses, high-resolution seismic and bathymetric surveys were performed. High-resolution seismic data allow the identification of different seismic facies and mainly transparent facies, which are usually interpreted as mass-transport deposits (Sammartini *et al.*, 2019). Bathymetric data allow the morphological identification of ablated areas, channelized deposits and slumps.

In a second step, new data are presented from Lake La Thuile sediment sequence THU10 on the 6.2 to 10.0 m Master Core Depth (MCD). The upper 6.2 m of data were previously published in Bajard *et al.* (2016). The aim is to compare the occurrence of major MTDs in the Aiguebelette and La Thuile sedimentary sequences.

To assess the possible palaeoseismological significance of these new data, the source and processes leading to the deposition of these two significant MTDs will then be discussed, considering their occurrence near or at the Younger Dryas/Early Holocene climatic transition. Then, our new data will be compared with published seismic profiles from the neighbouring lakes Annecy and Bourget (France), as well as with datasets coming from other regional lakes.

STUDY SITES

Geological settings

The study area encompasses different geological domains from the western Alpine domain to the south-east to the molasse basin and the Jura Mountains to the north-west. The structure is inherited from the Alpine compression that took place mainly during Mio-Pliocene times (Burkhard & Sommaruga, 1998; Sommaruga, 1999; Affolter & Gratier, 2004). Several active faults are recognized over the study area (Jomard *et al.*, 2017; Fig. 1). Among them, the Col du Chat, Culoz (Talling *et al.*, 2012) and Vuache faults (Baize *et al.*, 2011) have been studied extensively, highlighting active strike-slip deformations that

affect Quaternary morphologies and deposits. In addition to geological observations, both geodetic data and earthquake focal mechanisms highlight a general north-west/south-east orientation for both compression and shortening axes (Rabin *et al.*, 2018), resulting in dominant strike-slip to oblique thrust faulting (Mazzotti *et al.*, 2020; Larroque *et al.*, 2021) over the area. In addition, geodetic data also reveal a current and general uplift, ranging between 0.5 mm/yr near the studied lakes and increasing up to 2.0–2.5 mm/yr in the higher chain (Sánchez *et al.*, 2018, Sternai *et al.*, 2019).

The instrumental seismicity in the area appears mostly diffuse, even though some significant instrumental events could be related to the activity of the mentioned faults, such as the 1996 Epagny earthquake triggered along the Vuache fault (Mw = 4.9; Manchuel *et al.*, 2018). In addition, several damaging events are reported in macroseismic catalogues, for instance, more than twenty earthquakes of epicentral intensity greater than VII (MSK-64 macroseismic intensity scale) in the SISFRANCE database of historical seismicity (Jomard *et al.*, 2021). In the vicinity of the studied lakes, the strongest historical reported event is ‘the Bugey earthquake’, which occurred north of Lake Bourget in 1822 CE, probably along the Culoz fault, with an epicentral intensity of VII–VIII and an estimated magnitude of Mw = 5.5 ± 0.3 (Manchuel *et al.*, 2018). This event triggered an up to 19 cm thick homogeneity-type deposit revealed in sediment cores from Lake Bourget’s infill (Chapron *et al.*, 1999).

Lake Aiguebelette

Lake Aiguebelette (AIG) is a post-glacial peri-Alpine lake located in the inner Jura Mountains, on till and sandstone, between anticlines. Lake Aiguebelette is 373 m above sea level. Its surface area is approximately 5.45 km². The main tributary is the ‘Leysse de Novalaise’ entering the northern part of the lake. The lake catchment area of 70 km² is characterized by an area occupied by grasslands and cereal fields and pastures on the western side, contrasted with steep slopes covered by forests on the eastern flank of the ‘Chaîne de l’Épine’ mountain ridge (Fig. 2), where numerous rockfalls have been mapped. Three geological formations constitute the main source of sediment to the lake: Jurassic and Early Cretaceous limestones, Neogene sandy molasse and Quaternary Würmian tills (Fig. 2; Gidon, 1962). Lake Aiguebelette was overdeepened by glacier erosional action during the Würm period

(Coutterand, 2010). It can be divided into three subbasins of 29 m, 45 m and 71 m depths separated by two glacial rock sills (Fig. 2). One of these partially emerges as islets to the south (Jargot & Loup, 1983).

Lake La Thuile

Located in the south of the French sub-Alpine Bauges Massif at 874 m above sea level and 30 km away from Lake Aiguebelette, Lake La Thuile is a 0.0713 km², oval-shaped lake of glacial origin with a maximal water depth of 8 m (Fig. 3). There is an absence of steep slopes in Lake La Thuile and in its watershed. There is no evidence of major past gravitational movements. Two temporary streams enter the lake during

snow melt and long rainfall periods (Bajard et al., 2016). The lake catchment area of 1.6 km² is mainly forested, except for the grasslands and anthropized areas near the lake. According to the geological map (1/50 000), the catchment area is composed of carbonate rocks: Jurassic micritic limestones and Cretaceous marls, shales and spathic limestones (Gidon & Barféty, 1969).

NEW DATA AND METHODS

Bathymetry

A bathymetric survey was conducted in October 2017 in Lake Aiguebelette using a Reson 8101 multibeam echo-sounder (Teledyne Reson,

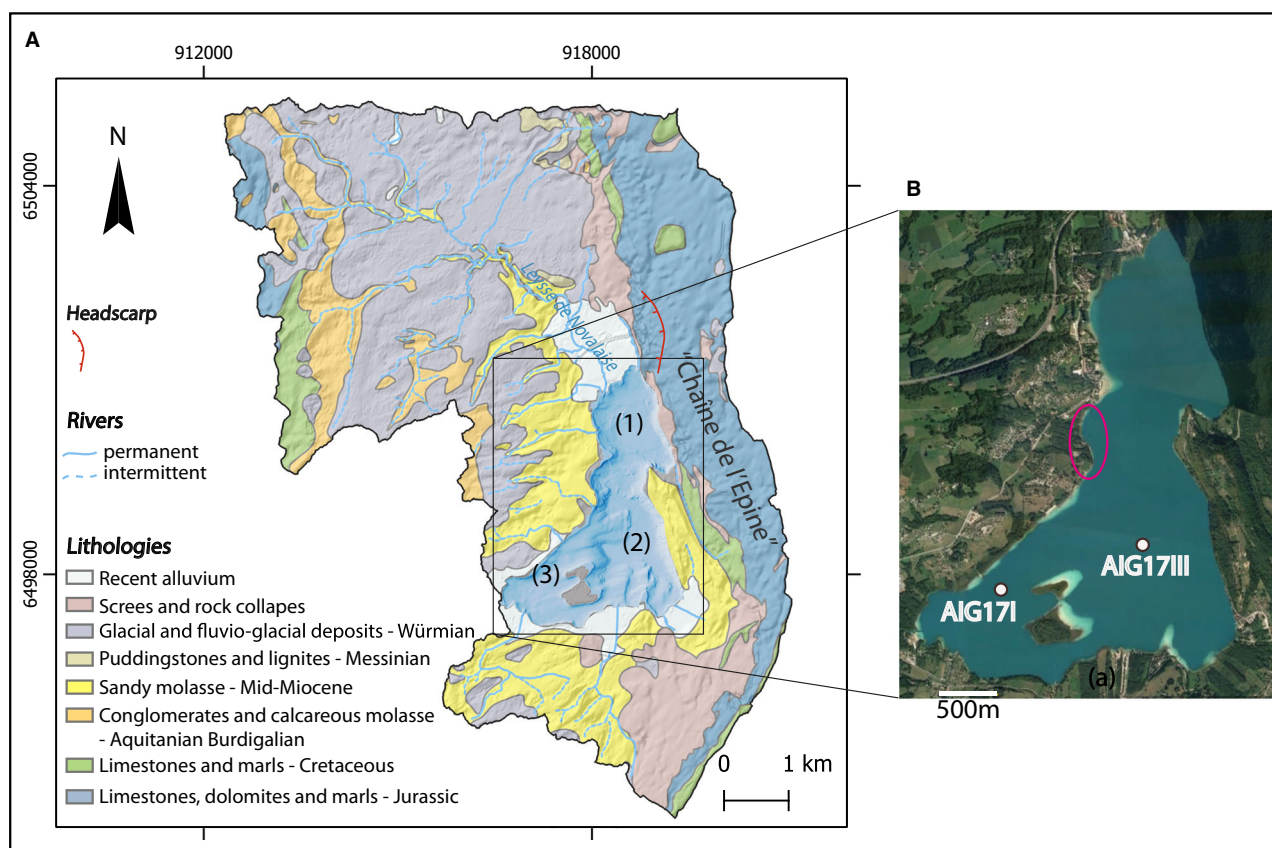


Fig. 2. Settings of Lake Aiguebelette (AIG). (A) Geology of the catchment area. Description and age of each geological layer from the BRGM 1/50 000 regional map. Projection: Lambert-93 (EPSG 2154). The three subbasins – (i) northern basin and southern (ii) deep and (iii) shallow basins – are indicated. The headscarp of the Nances landslide is indicated in red. Detailed bathymetry can be found in Appendix S1: SM3, Fig. SM1. (B) Aerial picture showing the surrounding lake. Coring locations of sediment sequences (AIG17I) in the shallow basin and (AIG17III) in the deep basin are displayed by the white dots. Note the occurrence of carbonates on the shallow slopes of the lake along the western coast (clear blue colour). The area circled in red shows an absence of carbonates (*Discussion* section).

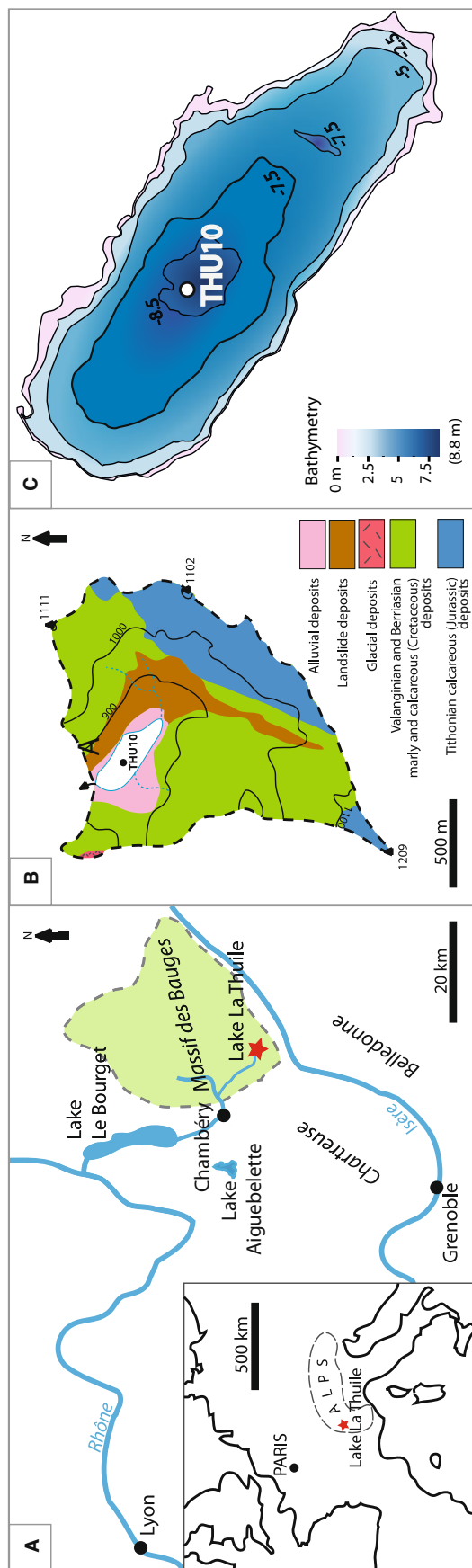


Fig. 3. Lake La Thuile in the Massif des Bauges, modified from Bajard *et al.*, 2016: (A) location; (B) geology of the watershed; and (C) bathymetry and coring location (white dot) of the THU10 sequence.

Slangerup, Denmark). Measurements were made in two phases, the first with a 1.5 by 2° beam width and 210 kHz frequency and the second with a 1.2 by 1° beam width and 400 kHz frequency. Between 0 m and 5 m depth, the maximum angular coverage (mac) was 120 to 130°; between 5 m and 20 m, mac was 110°, and below 20 m, mac was 90°. The absolute depth accuracy depends on the motion sensor's capability to compensate movements due to waves and positioning accuracy. The water depth accuracy is in the range of centimetres in shallow waters to a few decimetres at depths of >50 m. Data were acquired and processed by iXBlue company, with QINSy 8.15.0 software (QPS, The Netherlands).

A bathymetric survey was conducted in Lake La Thuile in December 2009 for ecological and piscicultural works by the private company 'SAGE environment' with a multibeam echosounder (200 kHz frequency and 4000 watts crest to crest). The positioning system (dual-antenna receiver Trimble BD982 GNSS system; Trimble, Sunnyvale, CA, USA) includes a 16-channel GPS receptor with centimetre accurate positions. Complementary spot measurements were acquired every 10 m on several transects.

Reflection seismic

A total of 17.5 km of seismic profiles were acquired in November 2020 in Lake Aiguebelette by the iXblue company. An Echoes 10 000 (5–15 kHz) chirp subbottom profiler (iXblue, Saint-Germain en Laye, France) designed for shallow water environments was used at 2 kVA power. A 10 ms pulse was emitted using frequency modulation of 5 to 15 kHz, thus delivering high-resolution (<8 cm) seismic data (CHIRP signal was processed for 10 ms for the total length signal). Seismic profiles were recorded in SEG-Y format using a global positioning system (GPS used is Garmin GNSS differential without RTK correction allowing a precision lower than 10 m) and processed with Delph Seismic software. Data processing involved digital subtraction noise filtering, water bottom mute and bandpass filtering.

Due to the shallow depth of THU Lake (8 m at its deepest point), no seismic survey was conducted here, as problems may arise with the almost simultaneous arrival of different wave types and the occurrence of multiples at a short time interval after the primary event.

Lake sediment coring and description

In Lake Aiguebelette, two sediment sequences were retrieved using a Uwitec platform and corers (Uwitec, Mondsee, Austria). The cores were collected before acquiring seismic data. The coring sites were determined based on the bathymetric map in two different subbasins far from the main tributaries to minimize the impact of potential flood deposits. In 2017, two cores were retrieved, including a *ca* 16 m long core named AIG17III in the deepest basin of Lake Aiguebelette (45.5503°N, 5.8015°E, at a water depth of *ca* 70 m; IGSN: TOAE0000000393 to TOAE0000000410) and a 10.4 m long core named AIG17I in the shallowest basin (45.5470°N, 5.7855°E, at a water depth of 26.9 m; IGSN: TOAE0000000380 to TOAE0000000390).

The sediment was retrieved from two (AIG17I) and three (AIG17III) parallel holes using 2 m long core liners of 90 mm in diameter. A depth offset (≈ 70 cm) was maintained for the second and third holes to ensure section overlaps. A short gravity core (AIG-20-pilote) was also taken to obtain a well-preserved sediment–water interface. The cores were split into two halves at the EDYTEM laboratory (Université Savoie Mont Blanc). Each half-section was described in detail, and pictures were taken. Lithological description of the sequence allowed the identification of different sedimentary facies and marker layers from the overlapping sections and was used to build two composite Master Core Depth (MCD) sequences.

The same methodology was applied to cores retrieved from Lake La Thuile, constituting the THU10 sequence (IGSN: IEFRA00BB) previously described in Bajard *et al.* (2016).

Sedimentological and geochemical analyses

Grain-size analyses

To determine grain-size distributions within the main event layers (ELs) and compare them to those of the continuously accumulated background sediments, the cores were sampled with a 2 cm sampling step (*r*). Depending on the encountered facies, the step-resolution, *r*, was decreased (i.e. sandy layer) or increased (i.e. transition between facies) with $1 \text{ cm} < r < 5 \text{ cm}$.

Analyses were conducted with a Beckman Coulter Life Science 13230 XR laser particle-size analyzer (Beckman Coulter, Brea, CA, USA) at the EDYTEM laboratory. To avoid flocculation, the sonication tool was enabled during measurements. Grain-size distribution datasets were

processed with MATLAB R2019b software. The sediment grain size in THU10 was determined at a 2 cm step resolution using a Malvern Mastersizer 2000G laser particle sizer (Malvern Panalytical, Malvern, UK). The sonication tool was used to avoid flocculation.

Geochemistry

Relative variations in major elements were measured continuously every 5 mm by X-ray fluorescence (XRF) using an Avaatech core scanner (Avaatech, Dodewaard, The Netherlands) at the EDYTEM laboratory. The XRF measurements were performed on split cores of the AIG17I, AIG17III and THU10 composite sequences covered with a 0.4 mm thick Ultralene foil. On the Lake Aiguebelette sequences, a first measurement run was performed with analytical settings at 10 kV and 0.1 mA for 30 s to detect lightweight elements such as Al, Si, P, K, Ca, Ti, Mn and Fe. A second run at 30 kV and 0.3 mA for 30 s allowed the detection of Br, Rb, Sr, Zr and Pb. Each power spectrum was transformed into intensities expressed in counts per seconds (cps). On the Lake La Thuile sequence (THU10), a first run at 10 kV and 0.1 mA for 10 s and a second run at 30 kV and 750 μ A for 30 s were used.

This paper represents the XRF data in log-ratios according to Weltje *et al.* (2015) to avoid the influence of the sediment matrix effect in the geochemical (XRF) data. The data presented in this paper are focused on the thickest event layer of the deep basin sequence.

Loss on ignition

Following the procedure of Heiri *et al.* (2001), loss on ignition (LOI) was measured at 550°C for 4 h and at 950°C for 2 h to estimate the organic matter (OM), carbonate and terrigenous content in the samples from the THU10 sequence. These results are available and described in Bajard *et al.* (2016) for the top of the sequence (0–6 m). The same methodology was applied to samples from greater depths in the THU10 sequence.

Magnetic properties

Rock magnetic measurements and analyses were performed at the CEREGE laboratory at Aix-Marseille University. U-channels were sampled from sediment cores of the AIG17III (deep basin) sequence.

Two types of artificial remanent magnetization were induced and measured on the sediments.

First, anhysteretic remanent magnetization (ARM) was acquired using a 100 mT alternating field with a superimposed 0.05 mT steady field. ARMs and their stepwise demagnetization at 10, 20, 30 and 40 mT were measured with a superconducting magnetometer (2G Enterprises model 760R) to determine the mean destructive field (MDF) (i.e. the field needed to destroy half of the ARM). Second, isothermal remanent magnetization (IRM) was created by successively passing the U-channels through Halbach rings imparting 0.3 T and 0.6 T magnetic fields. The field induced by the magnetized sediment was measured after each application of the field with a high-resolution magnetic scanner (Demory *et al.*, 2019).

To determine the anisotropy of magnetic susceptibility (AMS), 29 cubic samples were collected from the event layer and surrounding sediment in 8 cm³ nonmagnetic plastic boxes. The measurements were conducted with a magnetic susceptibility meter MFK1 (AGICO, Brno, Czech Republic) to determine the susceptibility tensor that can be represented by an ellipsoid with three eigenvectors (Kmax, Kint and Kmin). The AMS ellipsoid is assumed to reflect the preferred orientation of the magnetic grains in the sediments. According to Jelinek (1981), several parameters can be used, especially the magnetic foliation: $F = K_{int}/K_{min}$ has been used to characterize homogenite deposits (Campos *et al.*, 2013; Rapuc *et al.*, 2018).

Acoustic velocity measurements

To process seismic data with accurate sound velocity values, P-wave velocity was measured

on an upper interval (0 to 151 cm MCD). This interval was selected because it is representative of the Holocene facies. The unavailability of unopened cores representative of the Late Glacial facies in this sequence did not allow us to perform P-wave measurements on older sediments. Measurements were performed with a Discrete P-Wave (MSCL-DPW) benchtop instrument at the Chrono-environnement laboratory (Besançon University, France) designed to make precise measurements of P-wave velocity on rock or sediment samples.

Chronology

The chronology of the sedimentary sequences from Lake Aiguebelette's deep (AIG17III) and shallow (AIG17I) basins is based on nineteen and nine ¹⁴C AMS measurements of terrestrial macroremains (plant leaves, roots and seeds), respectively, performed at the Poznan Radiocarbon laboratory and Laboratoire de Mesure ¹⁴C (LMC14) ARTEMIS in Saclay (Tables 1 and 2).

Lake La Thuile's sediment sequence chronology is based on nineteen ¹⁴C AMS measurements of terrestrial macroremains. The Holocene age model was previously published by Bajard *et al.* (2016). This study presents four additional radiocarbon ages constraining the time of deposition of the sequence's base (THU10, Table 3).

The IntCal20 calibration curve was used for ¹⁴C age calibration (Reimer *et al.*, 2020) in the software R with package 'clam' (version 3.0.2; R Core Team, 2020). This package was used to generate an age/depth model (Blaauw, 2010) for

Table 1. ¹⁴C dates for AIG17I, calibrated with IntCal20 (Reimer *et al.*, 2020). Samples in bold correspond to rejected dates. All samples are terrestrial macroremains.

Sample name	Lab. code	Depth (mm)	Sample type	Age (BP)	Cal. min (cal. BP)	Cal. max (cal. BP)	<i>P</i>
AIG 17 I A01-1 W 124-125	Poz-118614	1245	Plant macroremains	270 ± 30	154	439	95
AIG 17 I B01-1 W 135	Poz-118615	2317	Plant macroremains	1580 ± 35	1390	1531	95
AIG 17 I A02-1 W 136-137	Poz-118616	3319	Plant macroremains	2475 ± 30	2373	2718	95
AIG 17 I B02-1 W 97-98	Poz-118617	4074	Plant macroremains	3600 ± 40	3730	4076	95
AIG 17 I B03-1 W 21-23	Poz-118618	5490	Plant macroremains	6210 ± 50	6979	7254	95
AIG 17 I B03-1 W 82-83	Poz-118971	6095	Plant macroremains	7950 ± 40	8645	8985	95
AIG 17 I A04-1 W 20.5-21.5	Poz-125958	6179	Plant macroremains	7760 ± 520	7668	9896	95
AIG 17 I A04-1 W 26.2-27.5	Poz-126027	6239	Plant macroremains	13 750 ± 70	16 413	16 940	95
AIG 17 I A04-1 W 53.5-54.5	Poz-126026	6509	Plant macroremains	8930 ± 70	9779	10 232	95

Table 2. ^{14}C dates for AIG17III, calibrated with IntCal (Reimer *et al.*, 2020). Samples in bold correspond to rejected dates.

Sample name	Lab. code	Depth (mm)	Sample type	Age (BP)	Cal. min (cal. BP)	Cal. max (cal. BP)	<i>P</i>
AIG16-08a 68-70	Poz-91100	731	Plant macroremains	80 ± 30	30	258	95
AIG16-08a 115	Poz-91101	1381	Plant macroremains	470 ± 30	493	540	95
AIG 17 III A02-1w 67	SacA 50487	2278	Plant macroremains (leaf)	1090 ± 30	932	1058	95
AIG16-08b 25-27	Poz-91102	2342	Plant macroremains	1115 ± 30	939	1174	95
AIG 17 III A02-1123.2	SacA 50484	2840	Plant macroremains	1600 ± 30	1408	1533	95
AIG16-08b 66-68	Poz-91103	3025	Plant macroremains	1640 ± 35	1411	1684	95
AIG 17 III B02-1w 108.9	SacA 50488	3759	Plant macroremains (leaf)	2055 ± 30	1929	2106	95
AIG 17 III A03-1w 38	SacA 50489	4127	Plant macroremains (leaf)	2530 ± 30	2495	2741	95
AIG 17 III A03-1100-101	SacA 50485	4752	Plant macroremains	3400 ± 30	3566	3813	95
AIG 17 III A03 1w 130.5	SacA 50493	5052	Plant macroremains	3760 ± 30	3990	4235	95
AIG 17 III A04-1w 19	SacA 50490	6029	Plant macroremains (leaf)	4720 ± 30	5325	5576	95
AIG 17 III A04-1 59-60	SacA 50483	6185	Plant macroremains	5305 ± 30	5955	6192	95
AIG 17 III B04-1w 30.2	SacA 50491	7075	Plant macroremains (tree bark)	6445 ± 30	7285	7426	95
AIG 17 III B04-1 58.7	SacA 57458	7073	Plant macroremains	7090 ± 40	7836	8008	95
AIG 17 III B04-1 77.5	SacA 50486	7548	Plant macroremains	6270 ± 35	7026	7269	95
AIG 17 III B04-1113.8	SacA 57459	7934	Plant macroremains	8725 ± 45	9548	9890	95
AIG17 III A05-1-34-35	SacA 53193	8371	Plant macroremains	9590 ± 45	10 753	11 153	95
AIG 17 III C05-1 81.7	SacA 57460	10 014	Plant macroremains	11 100 ± 50	12 896	13 108	95
AIG 17 III C05-1 88.3	SacA 57461	10 080	Plant macroremains	11 420 ± 60	13 173	13 424	95

each sedimentary sequence (AIG17III, AIG17I and THU10). Because the event layers in the sequence are interpreted as instantaneous deposits, it was mandatory to first build an event-free composite depth for each sedimentary sequence before generating the age-depth model. In each case, a smooth spline model was used [AIG17III: smooth parameter (*sp*) = 0.48; AIG17I: *sp* = 0.2; THU10: *sp* = 0.3].

RESULTS

Bathymetry and reflection seismics in AIG: morphology and stratigraphy

High-resolution seismic profiles were acquired across Lake Aiguebelette with dense coverage of the deepest basin (see Appendix S1: Additional

Figures, SM3 Fig. 1). In the deepest basin area, 3 km of profiles were analyzed. Acoustic velocities are based on mean P-wave values measured on a representative Holocene core section ($v = 1410$ m/s) in the AIG sediment sequence.

Above the low-reflection acoustic basement, the deepest basin is filled with up to 25 ms (two-way-time TWT) of sediment, equivalent to 15.2 to 17.6 m, based on the measured P-wave values. The sediment package can be divided into three seismic units. The Lower Unit consists of parallel, high-amplitude reflections with low-amplitude folding along the profile. The Middle Unit is a transparent layer contrasting with the Upper Unit in terms of facies. According to the P-wave value (1410 m/s), the thickness of this unit is *ca* 1 m. The Middle Unit is continuous at 500 m on a north–south axis (visible on profile 114516, Fig. 4) and at

Table 3. ^{14}C dates for THU10 sequences. Samples in bold correspond to rejected dates. Notice that several facies are similar at different depths.

Sample name	Lab. code	Depth (mm)	Sample type	Age (BP)	Cal. min (cal. BP)	Cal. max (cal. BP)	<i>P</i>
THU10-01A1b	SacA 24161	1000	Twigs and plant macroremains	250 ± 30	151	427	95
THU10-02A1a	Poz 41716	1970	Plant macroremains	6440 ± 180	6952	7660	95
THU10-01B1a	SacA 24162	2600	Twigs and plant macroremains	960 ± 30	792	923	95
THU10-02B1b	Poz 41624	3450	Reed fragments	1050 ± 30	917	1053	95
THU10-01C1b	SacA 24163	4500	Wood	1630 ± 30	1410	1567	95
THU10-01C1b	Poz 41625	4530	Wood	1650 ± 30	1414	1687	95
THU10-02C1a	Poz 41626	4850	Twigs wood and reeds	2525 ± 35	2493	2741	95
THU10-01C1b	SacA 24164	4990	Seed	2475 ± 30	2373	2718	95
THU10-01C1b	Poz 41627	5050	Seed	2840 ± 30	2865	3058	95
THU10-02C1a	SacA 24166	5100	Leaf (Fagus)	2835 ± 35	2856	3058	95
THU10-02C1a	Poz-51001	5240	Plant macroremains	3715 ± 35	3931	4215	95
THU10-02C1a	Poz-51002	5320	Plant macroremains	4440 ± 35	4878	5281	95
THU10-02C1a	Poz-44340	5590	Plant macroremains	6240 ± 40	7011	7257	95
THU10-02C1a	SacA 24167	5840	Peat	9110 ± 45	10 196	10 405	95
THU10-02C1a	Poz 41632	6210	Tree bark	10 220 ± 50	11 653	12 424	95
THU10-01D2b	Poz 41628	7480	Plant macroremains	11 230 ± 60	13 073	13 293	95
THU10-02D1b	SacA 24168	8380	Plant macroremains and seed	12 120 ± 60	13 804	14 122	95
THU10-01E1b	SacA 24165	9680	Plant macroremains, bark	12 580 ± 60	14 803	15 180	95
THU10-01F1a	Poz 41629	11 620	Plant macroremains, herbs, roots	13 580 ± 60	16 208	16 596	95

37.5 m on a south-west–north-east axis (profile 163358, Fig. 4). The Upper Unit is composed of parallel continuous reflectors with higher reflection amplitudes and a closer succession of reflections than the Lower Unit.

On bathymetric maps (Fig. 5), a geomorphological feature was observed that is channel-shaped. This feature is spread over 1 km with two main axes (north-west–south-east in the proximal part; north–south in the distal part). It extends from the midwestern slopes of the lake towards the deep basin (the most distal lobe still observable in bathymetric data is located 288 m north of the AIG17III coring point location) (Fig. 5B). Two east–west-oriented seismic profiles crossing the channel-shaped feature's southern distal lobe give an estimation of the levée bulge height (Fig. 5D). The bulges are inherited from the channel-shaped feature underlying the drape visible on both seismic profiles. The bulge height is estimated from the seismic profiles and ranges between 36 m and 152 cm.

Lake Aiguebelette deepest subbasin sediment data (AIG17III)

Stratigraphic unit descriptions

The following stratigraphic unit descriptions of AIG17III are based on macroscopic observations (facies) and XRF results.

The AIG17III sequence consists of clayey to silty finely laminated (<5 mm) sediment intermittingly interbedded with fifty-seven event layers with thicknesses ranging from 0.2 to 115 cm. Visual criteria allow identification of event layers such as turbidite (Tu), homogenite (Hm) or the succession of both (Tu + Hm). The homogenite (Hm) facies consists of a homogenous clayey (green to grey) sediment topped by a thin and clearer-coloured (often white) clay cap (Appendix S1: SM3 Fig. 4); the graded turbidite facies (Tu) consists of a poorly sorted (high standard deviation), normal graded deposit. Both facies contrast with background sediment. Between 0 cm and 21 cm and between 172 cm and 816 cm in the AIG17III sequence, a

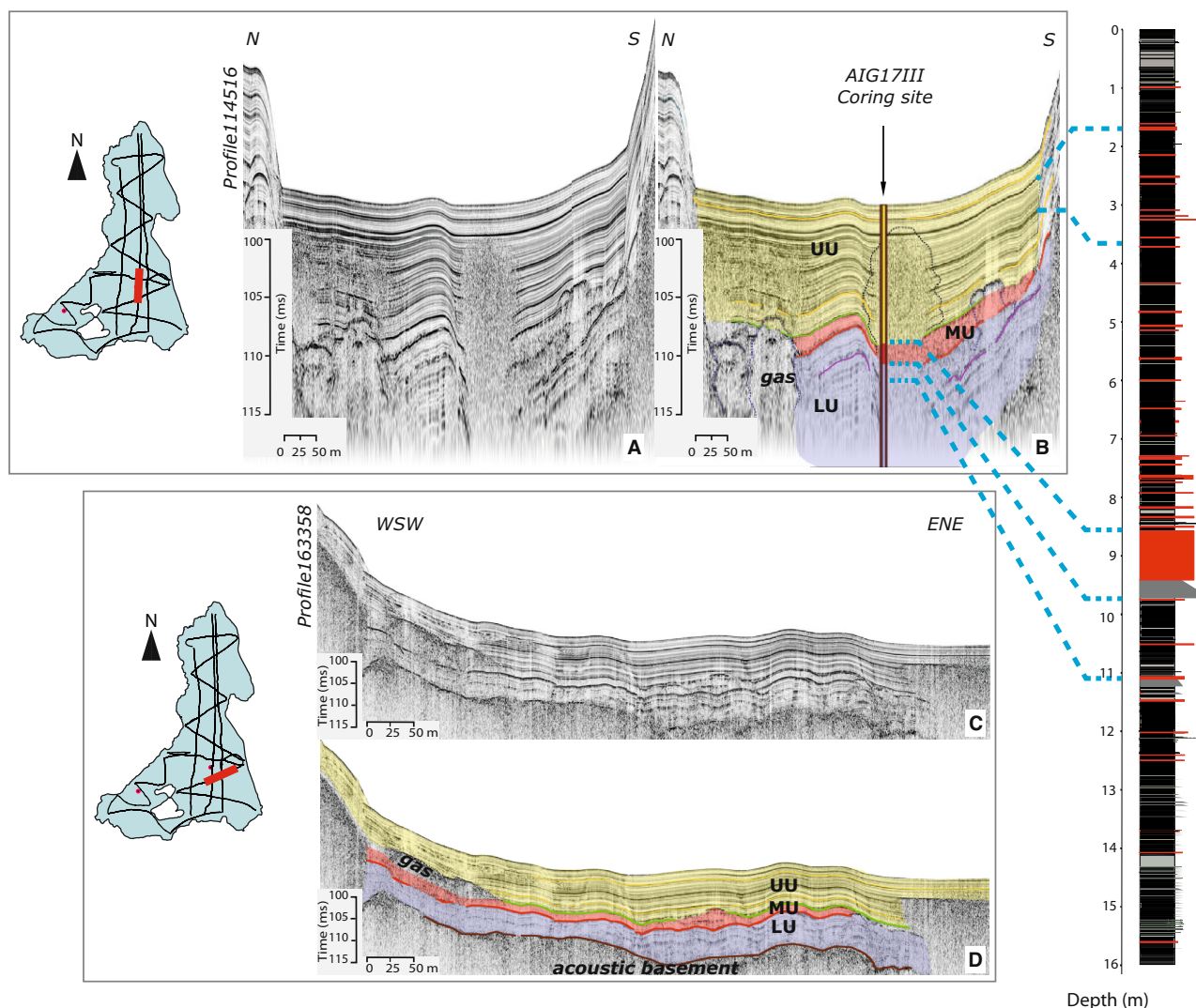


Fig. 4. Seismic reflection data from Lake Aiguebelette. (B) and (D) show the interpreted versions of the (A) and (C) seismic profiles, respectively. Plain brown lines indicate the top of the acoustic basement. The lower Unit 'LU' is highlighted in purple (B) and (D). The chaotic-transparent seismic facies from the Middle Unit 'MU' is interpreted in red. The Upper Unit 'UU' is highlighted in yellow. Reflectors at the base and top of the 'MU' have higher amplitudes and are highlighted by red and green lines, respectively, on the interpreted profiles. Gas blanking zones are contoured in thin dark-blue dotted lines. On the right, the simplified version of the AIG17III sediment sequence is correlated to seismic profile (B) by bold blue dotted lines.

characteristic alternation in the laminated facies was observed, including successive: (i) white; (ii) grey; and (iii) dark-grey to brown millimetre-scale laminae (Appendix S1: SM3 Fig. 4).

In AIG17III, eight different stratigraphic units were defined from the top to the bottom of the sequence (Table 4).

Grain-size analyses performed on the thickest event layer of the section confirm the homogeneous grain-size distribution of the Hm facies (Fig. 6).

Thickest event layer in the Lake Aiguebelette deep basin sequence

This section focuses on the thickest event layer archived in the Lake Aiguebelette deepest sequence and compares it to the surrounding sediment facies (continuous background sediment) characteristics.

The XRF data display higher $\ln(\text{Ca}/\text{Ti})$ contents in the event layer (Tu + Hm facies: mean of 5.1) than in the background sediment surrounding the event layer (mean of 4.6). In the graded base

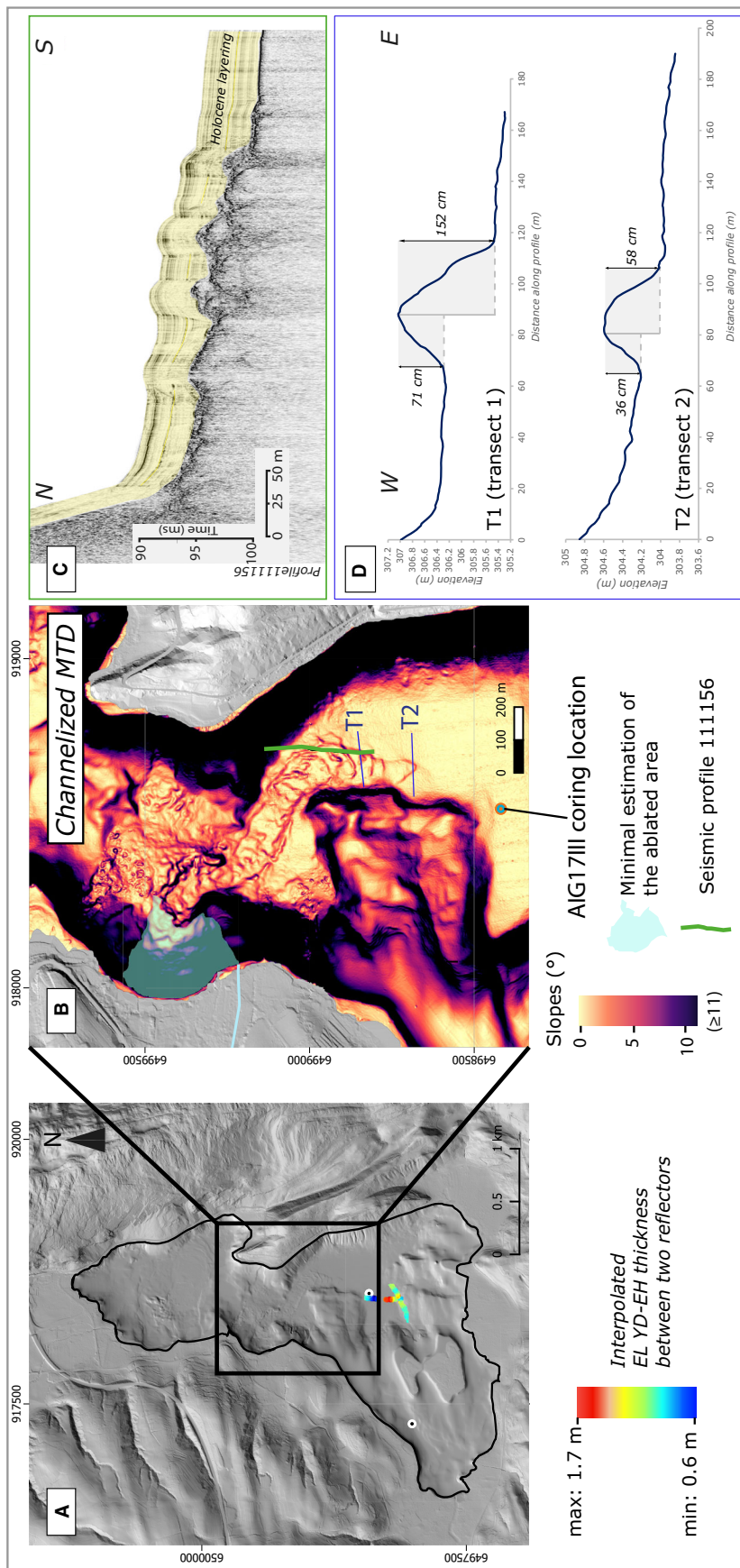


Fig. 5. (A) Digital elevation model and bathymetry of Lake Aigueblette. The colour gradient indicates the thickness of the Younger Dryas – Early Holocene (YD–EH) event layer estimated from seismic profiles 1114516 and 163358 (cf. Fig. 4). (B) Map of the slope angles derived from the bathymetric data with an enlarged image of a channelized deposit north of the AIG17III core point. Consecutive concentric bulges are visible along the channelized feature (bathymetric map). (C) North–south seismic profile 111156 crossing levées – location on map (B). (D) West–east transects T1 and T2 across the most distal head lobe – location on map (B).

Table 4. Description (units) of the sediment sequence AIG17III. MCD: master core depth.

Unit	Depth MCD (cm)	Description	Specific characteristics
1	0 to 21.0	Brown to greenish clays with alternations of type (1), (2) and (3) laminae	–
2	21.1 to 165.5	Grey to brownish clay with faint lamination	Topped by three silty layers (of 2 to 3 mm each); laminae are less diffuse from 104.5 to 165 cm MCD
3	165.5 to 374.2	Grey to brownish sediments with alternations of type (1), (2) and (3) laminae	Topped by a 5 cm thick visually homogeneous brown clayey to silty event layer (the thickest one observed in this unit)
4	374.2 to 513.9	Olive brown clays	Alternating thin clayey to silty dark sections and clear grey to yellow laminae
5	513.9 to 728.7	Thin clayey to silty layers of brown to greenish-grey with submillimetre-scale darker laminae	–
6	728.7 to 1150.3	Brown to greenish-grey clayey-silty sediment with millimetre-scale laminae	Part of this unit is composed of an event layer. This event layer is constituted by a 31.4 cm thick sandy graded base topped by an 83.6 cm thick homogenous deposit (Fig. 6). These two facies constitute the thickest (115 cm) event layer of the sediment sequence
7	1150.3 to 1410.7	Grey–brownish clay and silt with fine millimetre-scale dark and clear grey laminae with no specific repetitive pattern	Millimetric to centimetric-graded sandy event layers are observed in this unit
8	1410.7 to 1598.7	Clayey to silty grey and olive green sediments with thicker (several millimetres thick) laminae	The lower 70 cm are characterized by faint lamination

facies, the values are higher (mean of 5.2) than in the Hm facies (mean of 4.9), (Fig. 6).

The grain size of the continuous background sediment preceding the event layer is $3 \mu\text{m} < D50 < 5 \mu\text{m}$, $\sigma_{\text{SC}_D50} = 0.06$ and $11 \mu\text{m} < D90 < 13 \mu\text{m}$, $\sigma_{\text{SC}_D90} = 5.89$. Increasing D50 and D90 values are observed in the graded base, respectively, from 9 to 120 μm , $\sigma_{\text{GB}_D50} = 49.02$, and 130 to 150 μm , $\sigma_{\text{GB}_D90} = 92.25$, with the highest abundance of coarser material occurring at the base of the graded deposit. Grain-size values in the homogeneous facies range from $5 \mu\text{m} < D50 < 7 \mu\text{m}$, $\sigma_{\text{Hm}_D50} = 0.62$ and $25 \mu\text{m} < D90 < 64.5 \mu\text{m}$, $\sigma_{\text{Hm}_D90} = 5.46$. In the thickest event layer of Lake Aiguebelette's deep basin sequence, the Hm facies is slightly coarser than the background sediment facies, while the graded base is clearly different facies with coarser sediment.

The anisotropy of magnetic susceptibility foliation measured in the background sediment and in the graded base of the event layer is *ca* 1%, whereas it is *ca* 4% in the Hm facies (Fig. 6).

Along the event layer, ARM MDF data are ≤ 30 mT, whereas they are ≥ 30 mT in the continuous sedimentation. It was observed that ARM MDF values centred on 24.6 ± 0.5 mT in the Hm, on 10.2 ± 0.5 mT in the graded-base and on 41.2 ± 4.5 mT in the continuous sedimentation (Fig. 6). Induced IRM measured amplitudes are $\leq 0.4 \mu\text{T}$ in Hm only (Fig. 6). All of these magnetic parameters indicate important differences in terms of magnetic mineralogy and magnetic grain sizes in each facies.

Lake Aiguebelette shallowest subbasin sediment data (AIG17I)

The AIG17I sequence (seven sedimentary units) (Table 5) contrasts with the deep basin sequence in core AIG17III, with very few laminae in the upper part of the sequence (Table 4, Appendix S1: SM3 Fig. 4). In the AIG17I sequence, twenty-one event layers are identified based on the same criterion presented in the AIG

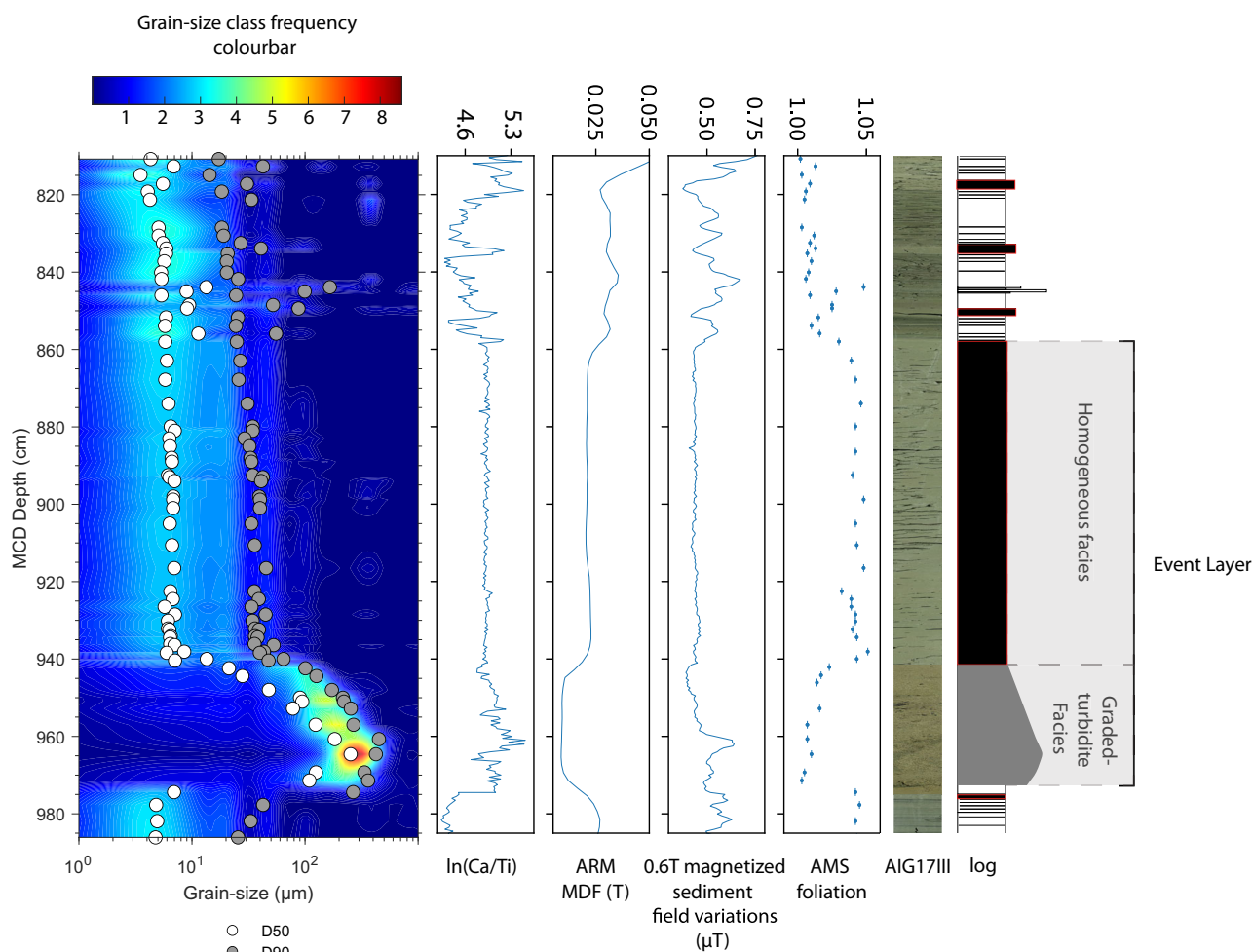


Fig. 6. Main sedimentological, geochemical and magnetic results at depths covering the large event layer of the AIG17III sequence. From left to right: grain-size measurements presented in a contourplot. D50 and D90 values are superimposed on the contourplot (white and grey dots, respectively); ln ratio; Mid-Destructive Field (MDF) of the Anhyseretic Remanent Magnetization (MDF ARM); magnetic field variations induced by the magnetized sediment (equivalent to low isothermal remanent magnetization; Demory *et al.*, 2019); Anisotropy of Magnetic Susceptibility (AMS) foliation; photography and macroscopic log description of the different facies types observed (plain black lines: laminated facies; black rectangles contoured in red: homogenite facies; grey graded symbol: graded turbidite facies with inverse-graded base topped with a main normal-graded facies).

deepest subbasin sediment data (AIG17III) section, with thicknesses ranging from 0.3 to 17.3 cm. Event layers are interbedded in the continuous sedimentation, mainly consisting of diffuse and sporadic laminae along the sequence.

Lake Aiguebelette sequences: chronology

Nine and nineteen ^{14}C measurements on terrestrial plant macroremains constrain the chronology and age-depth relationship of AIG17I and AIG17III sediment sequences from Lake Aiguebelette's shallow and deepest basins, respectively (Fig. 7).

One sample from each sequence was rejected after calibration to avoid age inversions (AIG17I, Table 1; AIG17III, Table 2). The rejection of these two samples allows the generation of an age-depth model with no major variation in the sedimentation rate. A possible explanation for the younger radiocarbon ages could be contamination during sampling.

These age models (Fig. 7) show that both sequences cover the whole Holocene period without hiatus and at least part of the Late Glacial, with sedimentation rates ranging downcore between 0.05 and 0.1 cm/yr post-11 500 cal BP and ≥ 0.1 cm/yr since 2000 yr cal BP.

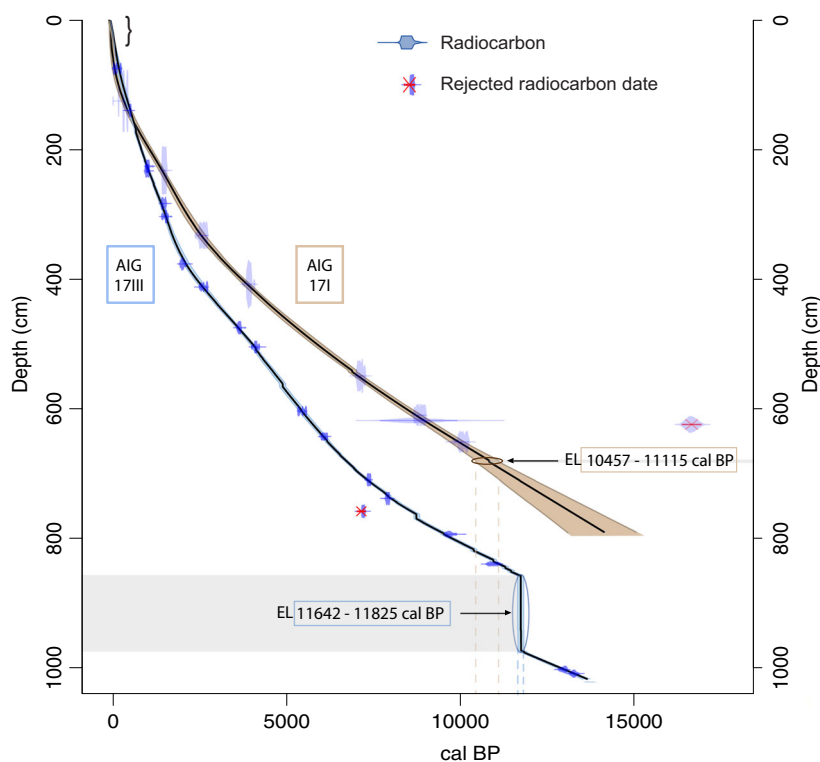


Fig. 7. AIG17III (blue) and AIG17I (brown) age-depth models. The Younger Dryas – Early Holocene (YD–EH) large event layer in the deep basin sequence is circled, and its depositional time range is marked by blue dashed lines. The EL of compatible depositional time archived in the shallow basin is circled in brown, and its depositional time range is marked by brown dashed lines.

Table 5. Description (units) of the sediment sequence AIG17I. MCD: master core depth.

Unit	Depth MCD (cm)	Description	Specific characteristics
1	0 to 185.7	Brown clay sediments	Faint and diffuse laminae in the upper 100 cm
2	185.7 to 483.8	Brown greyish clay with millimetre-scale laminae	Darker sediments between [227 to 258]; [332 to 399.8]; [407 to 414] cm MCD
3	483.8 to 554.5	Brown clayey to silty sediments	Faint laminae
4	554.5 to 625.5	Clear olive to grey clays with alternating dark and clear grey to yellow laminae sections	–
5	625.5 to 691.0	Clayey to silty brown to grey sediments with millimetre-scale laminae that are sometimes diffuse	–
6	691.0 to 823.4	Brown–greenish-grey clayey silty sediments with millimetre-scale laminae	Some layers are sandier and darker
7	823.4 to 1039.57	Brown to dark grey clay and silts	Marked by the presence of several millimetre to centimetre-scale sandy graded event layers and a major thick layer from 1022 to 1039.5 cm MCD with gravels and pebbles at its base

The large event layer in the deep basin sequence (AIG17III) has a depositional age that ranges between 11 642 and 11 825 cal BP with 95% confidence. In the same way, in the

shallow basin sequence, a 2 cm thick event layer occurs at a time range estimated between 10 457 and 11 115 cal BP (through extrapolation of the age-depth model) with 95% confidence and at

least older than 10 229 cal BP (maximum age of the last dated sample in the continuous sediment facies 27.2 cm above the event layer).

Lake La Thuile sediment data and chronology

The Lake La Thuile sequence is composed of 11 sedimentary units (facies units) mainly composed of clayey to silty material. These facies are

defined according to the sediment characteristics. The uppermost 620 cm of the THU10 sequence is fully described in Bajard *et al.* (2016). The present paper studies the lower part of this sequence, and focuses on an event layer. Four additional radiocarbon dates supplement the existing age-depth model of fifteen dates (Table 3) previously published in Bajard *et al.* (2016). In the THU10 sedimentary sequence, multiple repetitions of the same facies were observed (Fig. 8).

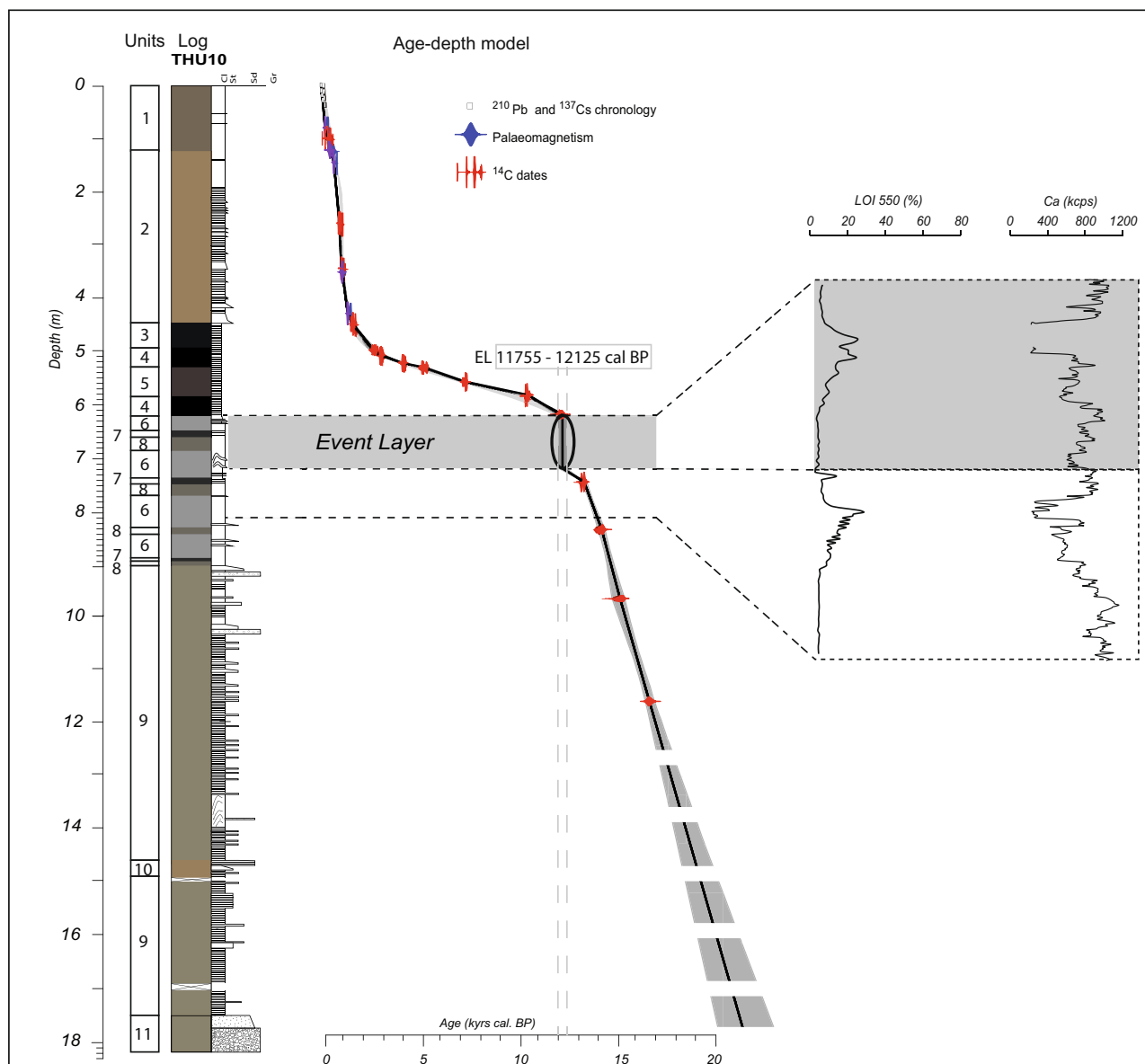


Fig. 8. THU10 main sedimentological and geochemical results. From left to right: THU10 sediment log; age-depth model including $^{210}\text{Pb}/^{137}\text{Cs}$ chronology (white rectangles); ^{14}C ages (red symbols) and palaeomagnetic secular variation constraints (blue symbols); loss on ignition 550°C; Ca content. From depths of 623 to 723 cm, an instantaneous deposit is evident.

The descriptions of facies 1 to 11 are summarized in Table 6. A particular repetition of the sediment interval is visible in the sequence: the interval between 623 cm and 723 cm MCD appears to be a repetition of the interval between 723 cm and 810 cm MCD. This is reinforced by the similar fluctuations in $\ln(\text{Ca}/\text{Ti})$ (XRF) and OM content and three sand layers in each part (Fig. 8). The only difference between the two intervals is the disturbed base of sandy layers (from 685 to 723 cm) in the lower part of the upper interval. This repetitive upper interval (between 623 cm and 723 cm MCD) is later interpreted as an event layer (EL) (see *Lake La Thuile event layer* section below and Appendix S1: SM3 Fig. 5). Between 623 m and 650 cm MCD, a clay to silty deposit topped with three normally graded sandy layers containing shell fragments was also observed. Compared to upper and lower sedimentation, this deposit has high $\ln(\text{Ca}/\text{Ti})$ and low OM (LOI 550 *ca* 10%). From 650 to 660 cm, a darker clay to silty deposit with three distinct dark laminae was found. These deposits hold higher OM

($15 \leq \text{LOI } 550\% \leq 30$) and relatively low Ca levels (Fig. 8).

The depositional chronology of the THU10 core sequence is constrained by nineteen ^{14}C measurements on terrestrial plant macroremains, short-lived radionuclides and palaeomagnetism. Short-lived radionuclide and radiocarbon ages of macroremains from the sedimentary sequence are available in Bajard *et al.* (2016) and reported in Table 3. Palaeomagnetic data are provided in Crouzet *et al.* (2019).

The deepest macroremain was found at 1162 cm MCD, yielding a radiocarbon date ranging between 16 200 and 16 600 cal BP (Table 3). The base of the sedimentary sequence is located 650 cm below this level and shows crystalline material of glacial origin. The oldest laminated lacustrine sediments should have been deposited immediately after the glacial withdrawal estimated to be approximately $18\,500 \pm 1500$ BP, according to cosmogenic dating (Wirsig *et al.*, 2016; Roattino *et al.*, 2022).

The event layer depositional time is constrained by a ^{14}C date from a sample taken from a

Table 6. Description (facies) of the sediment sequence THU10. MCD: master core depth. Notice that several facies are similar at different depths.

Facies	Depth MCD (cm)	Description	Specific characteristics
1 and 2	0 to 450	Light clay and silt	Described in Bajard <i>et al.</i> (2016)
3 to 5	450 to 623	Dark sediments with higher OM content and present intervals of millimetric lamination	Described in Bajard <i>et al.</i> (2016)
6	[623 to 648]; [685 to 735]; [768 to 827]	Light grey clayey to silty deposits	Punctual presence of darker, normal graded sandy levels with shell debris
7	[648 to 660]; [735 to 747]; [882 to 890]	Dark grey clayey to silty deposits	Three darker centimetric levels for the uppermost depth interval
8	[660 to 684]; [747 to 769]; [827 to 840]; [890 to 898]	Clayey to silty olive grey deposits occur with shell debris	See the detailed description in the <i>Lake La Thuile sediment data and chronology</i> section
9	[898 to 1465]; [1490 to 1748]	Light olive grey silty clay with laminae between fine silty-clay and sandy deposits	Presence of fine to medium coarse sands (shell and organic matter rich) as well as limestone gravels and angular pebbles
10	1465 to 1490	Silty to clayey yellowish-brown deposits with fine to coarser dark sands	Presence of organic matter occurs. The coarser material is composed of micaschists
11	1748 to 1818	Top: coarse sand; base: gravels and angular pebbles (some rounder than others), within a light olive grey clayey to silty hardened matrix	Pebbles are mainly limestones from the catchment but also crystalline material with quartz, micas and amphiboles, demonstrating their glacial origin

1 mm thick continuous sediment layer immediately above the event layer (which is the best available option to date the EL). This sample has a depositional time range of 11 755 to 12 125 cal BP. Given that this sample was taken 1 mm from the top of the event layer and, given the radiocarbon range of uncertainties, the authors assumed that THU10's main event layer was deposited between 11 755 and 12 125 cal BP.

DISCUSSION

Source and depositional processes related to the thickest event layer in Lake Aiguebelette

The thickest event layer evidenced in the AIG17III sedimentary sequence (115 cm thick) shows inverse grading (coarsening towards the top) within the first 10 cm (Fig. 6). This could be interpreted as a consequence of an upward velocity gradient combined with a laminar regime (Mulder & Alexander, 2001). Above it, a classical fining-upward pattern is present, indicating a decrease in the sediment flow velocity during deposition (Mutti *et al.*, 2009; Zavala & Arcuri, 2016). Compared to the entire normal graded base, the homogenous part of the event layer (i.e. Hm facies) is characterized by little variation in the D90 and D50 parameters (Fig. 6). This suggests that Hm deposition was mainly controlled by sediment settling rather than by flow velocity (Arnaud *et al.*, 2012; Wilhelm *et al.*, 2016). This type of event layer has been described as a 'turbidite + homogenite' (Tu + Hm) facies in marine environments (Campos *et al.*, 2013; de Gelder *et al.*, 2022).

In the Hm facies, an increase in AMS foliation was observed. High magnetic anisotropy suggests that specific hydrodynamic conditions prevailed during sediment deposition, which allowed the physical alignment of elongated or flattened grains (Tanty *et al.*, 2016). The homogenite facies is characterized by a flattening of the magnetic susceptibility ellipsoid (i.e. high foliation parameter), which could be interpreted as related to a seiche (Campos *et al.*, 2013; Petersen *et al.*, 2014; Rapuc *et al.*, 2018). Water mass oscillation in a lake may be induced by an earthquake (Campos *et al.*, 2013) and/or a large proximal aerial or subaquatic landslide (Kremer *et al.*, 2012; Hilbe & Anselmetti, 2014; Van Daele *et al.*, 2015). These processes can produce seismic ground motions and trigger aquatic landslides (cf.

discussion in the *Origins of the mass-transport deposits* section).

Based on correlations between the vertical thickness on the seismic profiles and AIG17III sequence units (Fig. 4), the seismic stratigraphy was interpreted as follows. (i) A 'Lower Unit' (LU) corresponding to sediments deposited during the Late Glacial where undulations follow the bedrock structure. (ii) A 'Middle Unit' (MU) highlighting a transparent facies overlying a high-amplitude reflector and corresponding to the AIG17III event layer at the YD–EH transition. Such seismic signatures have been interpreted from other lakes as MTD facies (Chapron *et al.*, 1996; Moernaut & De Batist, 2011; Bellwald, 2012; Kremer *et al.*, 2017). (iii) An 'Upper Unit' (UU) characterized by high amplitude and continuous reflectors of Holocene layered sedimentation. Acoustic masking cross-cutting seismic units are interpreted as caused by interstitial gas.

The AIG17III coring location (Fig. 5A) is located south of the channelized MTD observed in the bathymetry. The source area of this MTD was identified on the western flank of the lake by mapping landslide headscarps through GIS analysis of bathymetric data (Fig. 5). The volume of remobilized sediment generated by the MTD is estimated at *ca* 375 300 m³ through the reconstruction of a prefailure slope profile on the bathymetric data by kriging (surface used for kriging shown in Fig. 5B). The obvious question is whether the transparent seismic facies of the MTD and AIG17III YD–EH event layers represent common deposits from the same depositional event.

On the bathymetric map and the available seismic reflection profiles, it is not possible to follow the MTD from the frontal lobe, visible in the bathymetry, to the AIG17III coring location (Fig. 5B) due to a lack of information in this zone (gas). However:

- A north–south seismic profile crosses the south-eastern levée deposits of the MTD. On this profile, *ca* 3 m thick continuous Holocene sediment layering that drapes the levée bulges was observed. As the thicknesses of the southern distal lobes (maximal height measured in the bathymetry between 58 cm and 152 cm, Fig. 5D) are of the same order of magnitude as the thickness of the AIG17III sedimentary YD–EH event layer (115 cm) retrieved in the deep basin sediment sequence, the channelized MTD and the major event layer could correspond to the same event. In other seismic profiles (Fig. 3), a transparent

facies is positioned under the Holocene drape. This facies (Middle Unit) has been interpreted as an MTD.

- At the MCD (master core depth) immediately under the Holocene sediments in the AIG17III sediment sequence, a turbidite–homogenite (Tu + Hm) facies was observed. In the Hm facies, a higher Ca/Ti content suggests a Ca enrichment compared to the background sediment (located under and above the event layer) (Fig. 9). The source of this sediment could be the shallow coastal carbonate area on the western flank of the lake.

- The channelized deposit is visible in the bathymetric maps (see Fig. 5B). It is sourced from the western flank of the lake in a zone where coastal carbonates are not visible. However, coastal carbonates are present everywhere else on the western flank of the lake except where the channelized morphobathymetric feature is taking its source (Fig. 2).

- Using geochemical data (Fig. 9), it was observed that the slope of the relation between Ca and Ti is negative in the continuous background sediment above and below the event layer, whereas it is positive inside the YD–EH event layer, which suggests that the source of the event layer is different from the surrounding background sediments. This point also supports the possible origin of the event layer sediment from the western flank of the lake, which has more coastal carbonates (Fig. 2). In this case, deposition of carbonates during Late Glacial or Early Holocene periods should have occurred in Lake Aiguebelette, such as in Lake Le Bourget or in several other French lakes (Magny *et al.*, 2006).

Then, the assumption that the channelized MTD and YD–EH event layers reflect the same object seems reasonable. The MTD (Fig. 5) should have been strong enough to transport sediments downslope towards the deep basin. The transportation over the entire basin could have been induced by a change from plastic to fluidal behaviour of the flow, while slope angles decreased from the flanks to the bottom of the lake (Shanmugam, 2002).

Similarly aged event layers during the Late Glacial to Holocene transition

Lake Aiguebelette YD–EH event layers in the two southern basins

AIG age-depth models for the AIG17III sequence provide a time range between 11 642 and

11 825 cal BP for the thick event layer deposit. In the AIG17I sequence (shallow subbasin), the event layer is dated from 10 457 to 11 115 cal BP (Fig. 7). The chronology for the event layer in AIG17I, however, is less well-constrained because of the absence of any radiocarbon dates below the event layer (due to the absence of vegetal terrestrial macroremains). Age-depth models suggest that both event layers are located at or close to the transition between the Late Glacial deposits and the Holocene continuous background, known as the Younger Dryas to Holocene transition dated at 11 700 cal BP (Hoek, 2008). Despite the uncertainties in the ^{14}C ages and differences in the age-depth modelling between the cores, it is possible that the two similarly aged event layers were generated by the same triggering event. Because the cores were collected in two separated subbasins with different bathymetry, sedimentation rates and processes, there is no possible correlation. In the case of a unique triggering event, the sedimentation dynamics at the lake scale could have been impacted and could have generated a seiche as attested to by magnetic properties of the sediment in the deep subbasin.

Lake La Thuile event layer

In the sediment sequence of Lake La Thuile, visual, sedimentological and geochemical analyses show the superposition of identical sediment sequences separated by a disturbed horizon (Fig. 8). The upper one together with its disturbed base is interpreted as an event deposit. In this deposit, the top three sandy layers are thicker than the ones *in situ* (below the disturbed base). This result suggests that the translated sediment package was closer to the source of the sandy particles, i.e. closer to the lake shore.

The setting of the THU event layer can be explained as follows: (i) the initiation of a sliding surface located at the basal part of the event layer, where the failure surface forms in the vicinity of an interface between sandy layers and clayey facies, may have favoured the slip process and rotational slide (Locat *et al.*, 2014; Gatter *et al.*, 2021); and (ii) the displacement of the sediments from a shallower slope towards the deeper basin during translational sliding (mass movement that produces the translational sediment package), favouring the preservation of the upper part of the displaced sediments (Appendix S1: SM3 Fig. 4). Although Lake La Thuile is shallow (current maximum depth: 8 m, certainly 6 m deeper 12 000 years ago;

Bajard *et al.*, 2016) and the bottom is quite flat, other examples of mass movement are known in shallow lakes with moderate slopes, such as Lake Savine and Lake Negre (Sabatier *et al.*, 2017; Lefebvre *et al.*, 2021). Such mechanisms have also been evidenced in submarine environments by Mulder & Cochonat (1996) and Talling *et al.* (2012). Lacustrine studies on Lake Lucerne also document such a mechanism (Schnellmann *et al.*, 2005; Sammartini *et al.*, 2021).

Age-depth modelling constrains THU10 event layer deposition between 11 755 and 12 125 cal BP with a probability of 95% (Fig. 7). This time range corresponds approximately to the Younger Dryas – Early Holocene transition, similarly aged in comparison with the event layers found in Lake Aiguebelette.

Similarly aged events at a regional scale

Several major MTDs have been observed in other Alpine lakes in the YD–EH transition time range. Among them, Lake Annecy and Lake Bourget (at distances to Lake Aiguebelette of *ca* 60 km and *ca* 15 km, respectively) were studied using seismic reflection surveys (Beck *et al.*, 1996, 2001; Van Rensbergen *et al.*, 1998; Nomade, 2005; Beck, 2009; Arnaud *et al.*, 2012; Talling *et al.*, 2012).

In Lake Annecy, MTDs are mostly located in the northern part of the lake, where the active Vuache fault is evidenced (Beck *et al.*, 1996; Nomade, 2005; Beck, 2009; Talling *et al.*, 2012). They are located stratigraphically between Late-Glacial sediments and Holocene layering (Fig. 10B), which chronologically equates to the YD–EH transition (Beck *et al.*, 1996, 2001). In Lake Bourget, seismic profiles (BOseis1317, among others, Fig. 10A) acquired in the deepest basin suggest the presence of a major MTD (identified as the chaotic-transparent HDU – Hautecombe Disturbed Unit) (Chapron *et al.*, 1996; Van Rensbergen *et al.*, 1999; Talling *et al.*, 2012). In Arnaud *et al.* (2012), the maximum interpreted age of the HDU is 9900 cal BP. The stratigraphic position of the HDU (i.e. between Late-Glacial and Holocene sediments – precisely at the basal part of the Holocene drape) suggests that it occurred around the YD–EH transition, i.e. *ca* 11 700 cal BP (Chapron *et al.*, 1996, 2016).

Origins of the mass-transport deposits

According to the previous paragraph, major MTDs are observed at the regional scale around

the YD–EH transition. While a seismic origin has clearly been established for several Swiss lakes (Strasser *et al.*, 2013; Kremer *et al.*, 2020), this remains unsolved for lakes in the north-western French Alps. This study, however, found for Lake Aiguebelette that the major observed event layer is most likely associated with the occurrence of a seiche and MTD. Hence, two hypotheses will hereafter be discussed to explain the occurrence of similarly aged MTDs at the YD–EH transition in the studied lakes as well as a seiche effect in Lake Aiguebelette:

- Climate change at the YD–EH transition favoured the occurrence of major catastrophic gravitational movements in the lakes' vicinity and/or the triggering of major MTDs within lakes;
- Regional stress modifications induced by local mass transfers (glacier melt and subsequent erosion) or broader scale glacio-isostatic uplift, favoured the release of seismic energy.

Gravitational movements

Less than 1 km from the north-eastern shore of Lake Aiguebelette, a major rockslide locally known as the 'Nances collapse', affects the Jurassic limestone series of the western subvertical flank of the Montagne de L'Épine anticline (Fig. 2). Its head scarp reaches 800 m, its total height reaches 430 m, and it is 1.5 km wide. At the foot of the slope, the deposit thickness exceeds 35 m. Assuming that it occurred at the YD–EH transition, could this event have triggered a major MTD in the lake as well as a seiche and hence be the source of the thickest event layer archived in the deep basin? Can such events also have occurred in the neighbourhood of other regional lakes highlighting major MTDs at the YD–EH transition?

The rationale behind these questions is that both slope debuttressing (Pellegrini *et al.*, 2006; Cossart *et al.*, 2008; Geertsema & Foord, 2014; Chiarle *et al.*, 2021) and permafrost melting (Noetzi *et al.*, 2003; Bodin *et al.*, 2015; Deline *et al.*, 2021) are known to be significant factors in triggering slope failures. Several major rock-fall events have, for instance, been associated with such effects (Gruber *et al.*, 2004; Huggel, 2009; Pirulli, 2009). Additionally, within the lakes, under-consolidation and excess pore pressure due to excessive sediment load in a short period of time (Prior *et al.*, 1982) may increase the lake's sensitivity to the triggering of

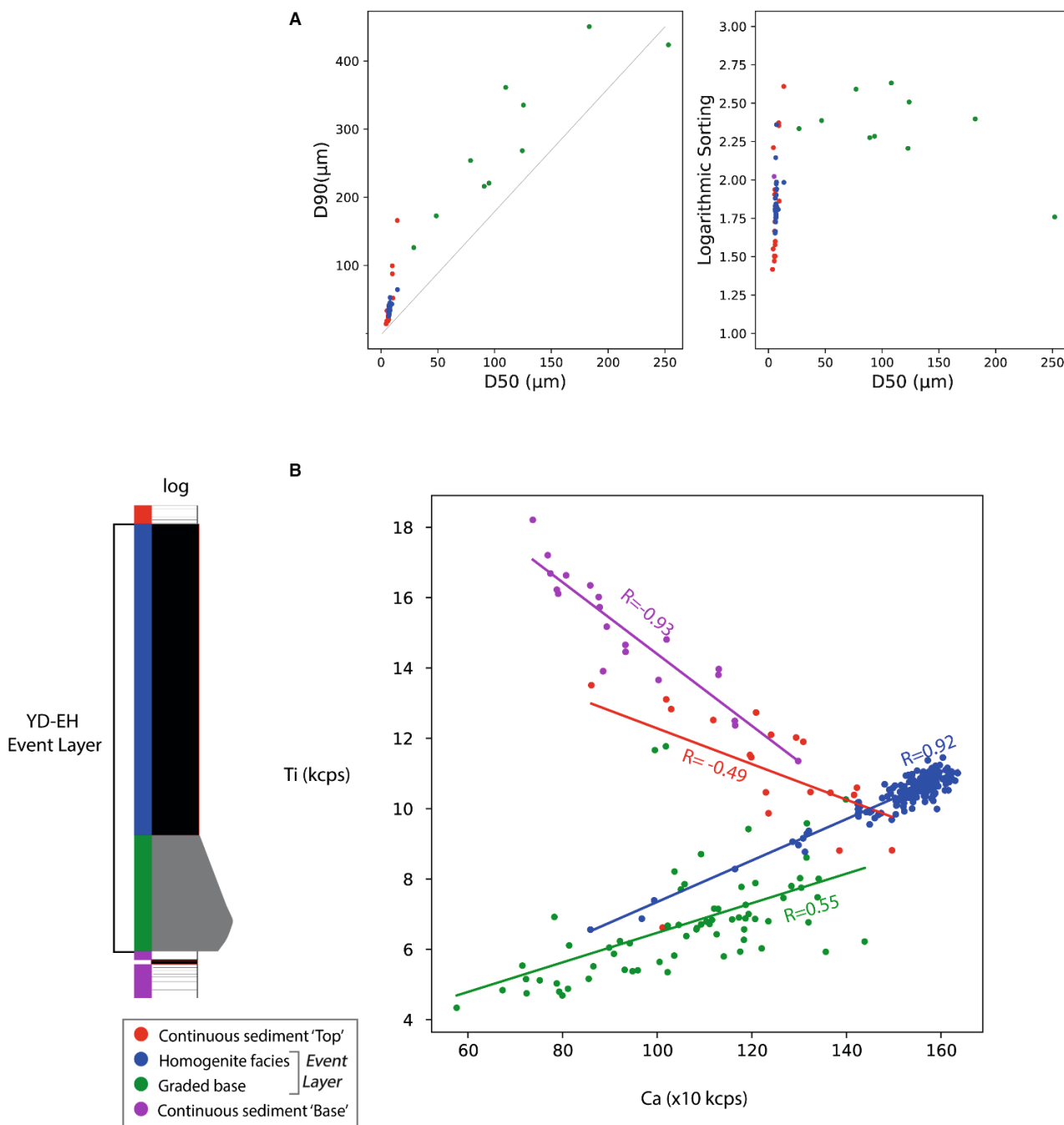


Fig. 9. (A) Passega-type diagram (D90 versus D50 and logarithmic sorting versus D50). Green dots: grain-size data of the upward-graded base; blue dots: grain-size data of the homogenite constituting the Younger Dryas – Early Holocene (YD–EH) event layer [which is interbedded in background sediments (magenta dots: grain-size data of the background sediments below the event layer; orange dots: grain-size data of the background sediments above the event layer)]. (B) Ti versus Ca diagram. Elemental X-ray fluorescence (XRF) data from the background sediments below the YD–EH event layer (purple dots); background sediments above the YD–EH event layer (orange dots); the graded base of the YD–EH event layer (green dots) and the homogenite facies (blue dots). R: correlation coefficient for each facies.

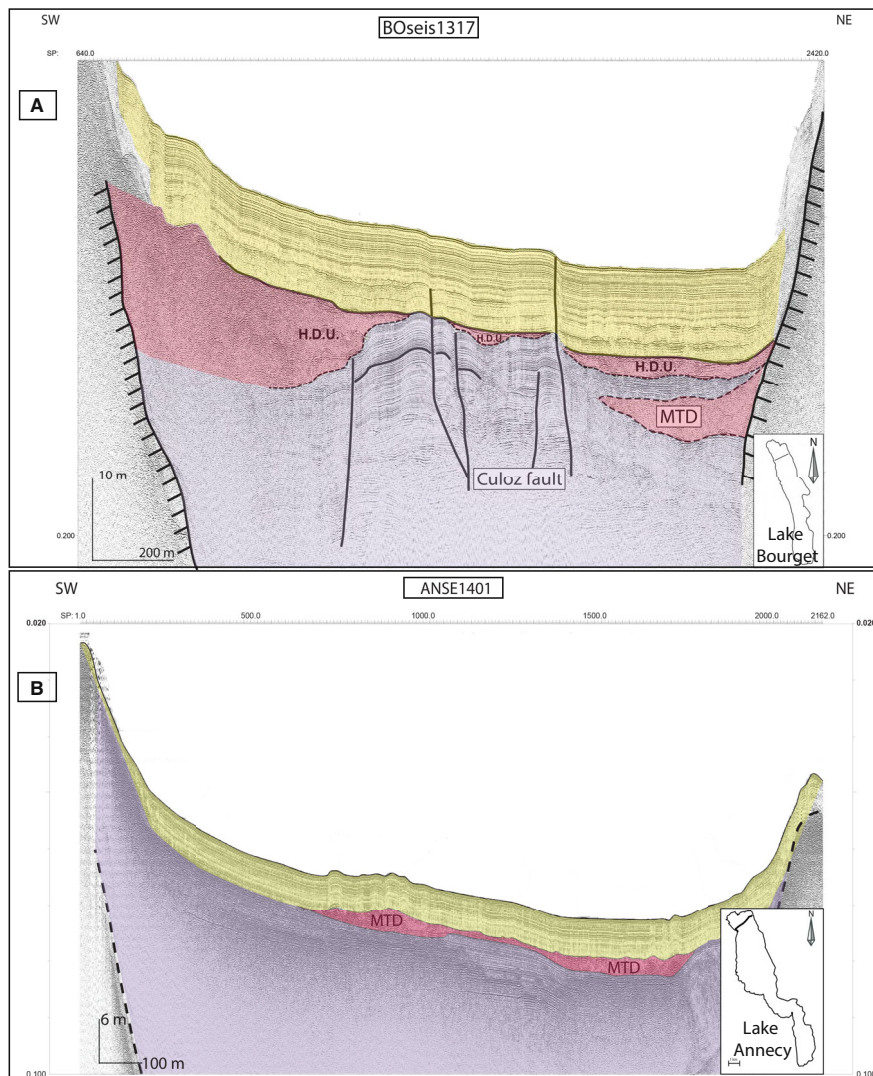


Fig. 10. Seismic profiles illustrating mass-transport deposits in two Alpine lakes, modified from de La Taille *et al.* (2015). (A) BOseis1317 seismic profile from the northern part of Lake Bourget. (B) ANSE-1401 south-west-north-east seismic profile from the northern part of Lake Annecy. In both profiles, the Lower Unit (purple) represents Late-Glacial sediments, whereas the Upper Unit (yellow) represents Holocene sediment draping. Between the units, the transparent-chaotic lenses (highlighted in red) correspond to mass-transport deposits (MTDs).

MTDs. Hence, seismic waves generated by rock-slides would be capable of triggering MTDs in lakes, especially if the lake sediments are more prone to destabilization. Finally, gravitational movements reaching the lakes can also produce major MTDs, as was shown in the nearby Lake Geneva. In this lake, the 563 AD turbidite resulted in a delta collapse triggered by the major Tauredunum rockfall (Kremer *et al.*, 2015).

Even though rockfalls are able to generate seismic waves (Lin *et al.*, 2015; Manconi *et al.*, 2016), these waves are known to attenuate

greatly with distance (Deparis *et al.*, 2008). Additionally, according to Blasio *et al.* (2018), the maximum equivalent magnitude of the energetic Cengalo rockfall (10^6 m^3) is approximately 3. Hence, their effect must only be very local and not affect other lakes at significant distances. For instance, the 1248 CE major Mount Granier collapse ($\approx 5.10^9 \text{ m}^3$ of rock displaced, around 13 km and 12 km away from Lake Aiguebelette and from Lake La Thuile, respectively) (Pachoud, 1991; Nicoud *et al.*, 1999; Blasio *et al.*, 2018) did not induce any significant (>10 cm thick) MTD in the studied lakes.

Furthermore, the close environment of other lakes from the study area (La Thuile, Bourget and Annecy) does not present any evidence of major catastrophic rockfalls capable of inducing significant and widespread MTDs. As a consequence of the above observations, the hypothesis of an enhanced occurrence of near-field major rockfalls as a source process to the event layer evidenced in the different sediment sequences presented here is very unlikely.

Seismic activity

Covering long timescales and wide areas, glacioisostatic adjustment (GIA) following deglaciation leads to surface uplift with subsequent crustal stress changes and potentially increased seismotectonic activity. However, it is unclear whether such a mechanism is needed to explain the contemporary earthquake activity in former glaciated shields (Stewart *et al.*, 2000) or if it plays a minor role (Bungum *et al.*, 2010). At more regional scales, however, it is well-established that the release of seismic energy may be temporarily enhanced (during a few kyr) along faults by local transient stress changes related to ice melting (e.g. Turpeinen *et al.*, 2008). Indeed, palaeoseismic evidence of post-glacial fault activity has been evidenced in several former glaciated shields, particularly in Fennoscandia, where 100 km long faults generated up to 7 m of coseismic displacement during $M_w \geq 7.5$ earthquakes (Mörner, 2004, and references therein).

In lacustrine palaeoseismology, however, there is not direct access to the seismogenic source responsible for the occurrence of MTDs, and it is difficult to decipher whether a specific seismically triggered MTD could have been triggered by a stronger and more distant earthquake or by a weaker and closer one. Concerning the studied region, similarly aged events may be:

1 Indicative of the occurrence of a major regional seismic event (Scenario 1) Such a hypothesis has, for instance, been tested by Strasser *et al.* (2006), who determined the necessary source parameters of an earthquake to produce multiple MTDs in lakes Zürich and Lucerne in Switzerland (≈ 300 km east of our study area). Based on the assumption that a macroseismic intensity of VII is required to trigger basin-wide landslides in Swiss lakes, they were able to identify three earthquakes of $M > 6.5$ – 7.0 , dated at 2.2, 11.6 and 13.7 kyr cal BP.

2 Indicative of the occurrence of lower-magnitude earthquakes in the close vicinity of

each of the lakes containing the similarly aged event layers/MTD (Scenario 2). To the authors' knowledge, such a hypothesis has thus far never been tested.

In the NW Alps and particularly in the study area, there is neither historical nor palaeoseismological evidence of the occurrence of an $M > 6.5$ earthquake. Regional studies conducted along regional active faults highlight relatively short and highly segmented fault systems (Jomard *et al.*, 2017), which tend to restrain the occurrence of higher-magnitude earthquakes (considering that fault length and magnitude are proportional parameters, e.g. Wells & Copper-smith, 1994). In addition, evidence of palaeoearthquakes affecting the ground surface is lacking or is at least tenuous, such as that observed along the Vuache fault (Baize *et al.*, 2013; Bellier *et al.*, 2021). Therefore, the authors consider Scenario 1 as being the most unlikely, even though one cannot discard the occurrence of a major event along a blind structure at depth (i.e. without identifiable surface rupture), as proposed by Strasser *et al.* (2006).

In Scenario 2, weaker earthquakes would have to occur closer to the lakes where the event layers were generated. In this case, the 1822 CE $M = 5.5 \pm 0.3$ earthquake (Manchuel *et al.*, 2018) could be considered as a reference event for discussion. This event occurred near the northern edge of Lake Bourget, triggering a significant event layer within the lake (Chapron *et al.*, 1999; Beck, 2009) and possibly a seiche, as reported by archbishop Billiet (1851). However, no major deposit could be associated with this event in Lake Aiguebelette, located 25 km south. Then, if it is considered that a $5 < M < 6$ earthquake occurring within a 25 km radius around each lake is required to produce significant MTDs, one could approximate the return period of such events based on published contemporaneous earthquake rates (Table 7). These have for instance been established by Drouet *et al.* (2020) for seismic hazard calculations. Gutenberg-Richter parameters established from seismicity catalogues for the region encompassing the studied lakes allow the estimation of the actual recurrence rate of a $M_w \geq 5.5$ at 0.58 events/year and of a $M_w \geq 6$ at 0.36 events/year and per million km^2 . This allows the estimation of the return period of an earthquake of $M \geq 5$ and an earthquake of $M \geq 6$ roughly between 400 and 1300 years within a 25 km radius of each lake (which should probably be an upper

Table 7. Estimation of the return period for a seismic event of M (magnitude) = 5; $M \geq 5.5$ and $M \geq 6$. In each case, the estimation is made as the seismic event was to happen within two areas centred on each lake location; in italics: within a circle of 10 km radius and in bold: within a circle of 25 km radius.

	M5	$M \geq 5.5$	$M \geq 6$
Regional earthquakes recurrence rate (established for 1.10^6 km ²) Drouet <i>et al.</i> (2020)	0.82 event/year	0.58 event/year	0.38 event/year
Rate near AIG for an area of			
≈ 355 km ²	<i>0.0002911 event/year</i> <i>(3435 years)</i>	<i>0.000206 event/year</i> <i>(4857 years)</i>	<i>0.000349 event/year</i> <i>(7413 years)</i>
≈ 2300 km ²	0.001866 event/year (536 years)	0.0013 event/year (769 years)	0.00087 event/year (1149 years)
Rate near THU for an area of			
≈ 273 km ²	<i>0.0002386 event/year</i> <i>(4467 years)</i>	<i>0.00015834 event/year</i> <i>(6316 years)</i>	<i>0.0001037 event/year</i> <i>(9639 years)</i>
≈ 2000 km ²	0.00164 event/year (700 years)	0.00113 event/year (885 years)	0.0007565 event/year (1321 years)
Rate near BOU for an area of			
≈ 683 km ²	<i>0.00056 event/year</i> <i>(1786 years)</i>	<i>0.000396 event/year</i> <i>(2524 years)</i>	<i>0.0002595 (3853 years)</i>
≈ 3000 km ²	0.00246 event/year (406 years)	0.00169 event/year (590 years)	0.00113478 event/year (881 years)
Rate near ANN for an area of			
≈ 543 km ²	<i>0.0004453 event/year</i> <i>(2246 years)</i>	<i>0.00031494 event/year</i> <i>(3175 years)</i>	<i>0.00020634 event/year</i> <i>(4846 years)</i>
≈ 2700 km ²	0.002214 event/year (452 years)	0.001526 event/year (655 years)	0.00102130 event/year (979 years)

limit considering the 1822 earthquake case) and between 1500 and 9000 years for a 10 km radius (Table 7). This means that the probability of producing similarly aged significant MTDs in regional lakes is low. As a consequence, if this second hypothesis is valid, it implies that earthquake rates at the YD–EH transition might have been higher than those calculated from current earthquake catalogues.

Perspectives at a broader scale

From the regional analysis herein, the authors propose that the occurrence of more frequent moderate earthquakes at the YD–EH transition could lead to similar effects in lakes in comparison with few regional major earthquakes.

From a sedimentological perspective, a first step would be to test this hypothesis at a broader Alpine scale, where numerous data are available in the literature. For instance, in lakes located in central Switzerland, several MTDs were deposited around the same period of time. Seismic data from Lake Zurich (Strasser, 2008; Kremer *et al.*, 2020), Lake Lucerne (Schnellmann, 2004; Becker *et al.*, 2005) and Lake Seelisberg (Monecke *et al.*, 2006; Strasser *et al.*, 2013) suggest similarly aged MTD events at *ca* 11 600 and *ca* 11 530 cal BP. At a broader scale in the Alps, several MTDs have been found in Lake Achensee (Austria), with ages ranging between 11 000 and 18 000 cal BP (Oswald *et al.*, 2022).

Beyond the Alps, other studies based on seismic data analysis suggest an archive of MTDs in

lake sediments at the YD–EH transition. For example, in the infill of the glacial lake Windermere (UK), seventeen MTDs (with a volume ranging between 2100 m³ and >100 000 m³) have been identified (Lowag *et al.*, 2012). Among them, fifteen were deposited at the transition between the Younger Dryas and the Holocene stages, whereas only two were deposited during the Holocene (Lowag *et al.*, 2012). While Vardy *et al.* (2010) postulated that the emplacement of these MTDs at the YD–EH transition may have solely been caused by slope overloading due to an increase in terrestrial sediment run-off, Lowag *et al.* (2012) observed the presence of fluid escape in the lake sediments, potentially linked to a period of increased seismic activity, prior to the Holocene stage.

Hence, to test our hypothesis a comparison with data coming from other former glaciated areas must be done (in particular with regions located closer to the poles, where the timing of the deglaciation is different from the Alps). Such a comparison may also help in deciphering processes involved in triggering seismicity.

In Fennoscandia and in the Laurentide, increased seismicity subsequent to ice melt following the Last Glaciation has been evidenced (Hasegawa & Basham, 1989; Nikolaeva *et al.*, 2016), as well as palaeoseismic events occurring at the last stage of the glacial age (Ojala *et al.*, 2019; Brooks, 2020). For instance, a major palaeoseismic event occurred in Lake Vättern (Sweden), at the YD–EH transition (Jakobsson *et al.*, 2014). Lake sediments recorded ≈13 m of coseismic displacement, consecutive to an earthquake of moment magnitude estimated at ≈7.5, being one of the largest known intraplate seismic events in Scandinavia.

Intensified ground shaking and rapid emplacement of mass movement deposits at the end of the Younger Dryas might have been facilitated by rapid climatic changes in several places around the globe (Lowag *et al.*, 2012; Forsberg *et al.*, 2016; Brooks, 2018; Sammartini *et al.*, 2019). At a large scale, climatic processes leading to warmer and wetter conditions can make subaqueous slopes unstable and preconditioned for failure. This might be reinforced by rapid deposition of unconsolidated sediment due to large sediment discharges during ice retreat (Forwick & Vorren, 2002; Nygard *et al.*, 2007; Clark *et al.*, 2010; Delaney & Adhikari, 2020). At the YD–EH transition, driving mechanisms leading to the deposition of MTDs in lake sediments and increased seismic activity

seem to be related to rapid deposition of unconsolidated sediment and regional changes in tectonic constraints subsequent to long-term isostatic uplift and transient perturbations related to mass transfer.

CONCLUSION

The multiproxy approach applied to the sediment sequence retrieved from Lake Aiguebelette's deepest basin allowed this study to highlight the presence of a 115 cm thick event layer, which is constituted by a turbidite–homogenite facies succession. It is highly likely that this event layer originates from a channelized mass-transport deposit (MTD), visible from the bathymetric and seismic data. Age models based on radiocarbon dates constrain the depositional age of the event layer to some time between 11 642 and 11 825 cal BP, which coincides with the Younger Dryas – Early Holocene (YD–EH) abrupt climatic transition. A similarly aged event layer may have been deposited in the shallow basin of Lake Aiguebelette between 10 457 and 11 115 cal BP. This time window (given the radiocarbon dates and age-depth model uncertainties) highlights the possibility of a single, common triggering source phenomenon for both events (at the scale of Lake Aiguebelette). Among several possible explanations, a seismic origin is favoured, supported by sedimentological analysis, and in particular by a high foliation of the anisotropy of magnetic susceptibility in the event layer interpreted as the consequence of a seiche in the lake.

At a regional scale a new MTD at the YD–EH transition in lake La Thuile, was also observed (depositional time range: 11 652–12 426 cal BP). In Lake Annecy and Lake Bourget, available published datasets show transparent seismic facies indicative of major and multiple MTDs underneath the Holocene sediment infill. Hence, the extent and occurrence of major MTDs in the study area at the YD–EH transition suggest a strong influence of this abrupt climate transition.

From seismotectonic data available in the region, the authors propose that the evidenced event layers may be related to moderate nearby seismic events rather than from the occurrence of large regional events. This hypothesis however implies that seismicity rates were higher than those observed in the history. In light of

this, warming climate during the Late Glacial, subsequent deglaciation, mass transfer and stress rearrangement may have been possible triggers of transient and increased seismicity rates.

ACKNOWLEDGEMENTS

This work was conducted as part of a PhD project funded by a joint grant from the University Savoie Mont Blanc and Institut de Radioprotection et de Sûreté Nucléaire. The acquisition of bathymetric data would not have been possible without Conservatoire des Espaces Naturels de Savoie, CCLA and Réserve Naturelle Régionale du Lac d'Aiguebelette. ¹⁴C analyses were acquired thanks to the CNRS-INSU ARTEMIS national radiocarbon AMS measurement programme at Laboratoire de Mesure 14C (LMC14) of the CEA Institute at Saclay (French Atomic Energy Commission). We are grateful to iXBlue for their help in acquiring seismic reflection data and providing access to DELPH interpretation software. We thank the EDYTEM sedimentology lab team for providing constant support and help in retrieving the sediment cores. We give special thanks to Thibault Roattino for his help in the use of GIS kriging methods. We also want to give a special thanks to Céline Beauval for our helpful discussions and models regarding regional seismicity rates. We acknowledge the Chief Editor Piret Plink-Björklund, Associate Editor Nathan Sheldon, Marc de Batist, and anonymous reviewers for their very helpful comments on earlier versions of the manuscript.

DATA AVAILABILITY STATEMENT

The data that supports the findings of this study are available in the supplementary material of this article.

REFERENCES

Affolter, T. and Gratier, J.P. (2004) Map view retrodeformation of an arcuate fold-and-thrust belt: the Jura case. *J. Geophys. Res. Solid Earth*, **109**, 1–20.

Alsop, G.I., Marco, S., Weinberger, R. and Levi, T. (2016) Sedimentary and structural controls on seismogenic slumping within mass transport deposits from the Dead Sea Basin. *Sediment. Geol.*, **344**, 71–90.

Arnaud, F., Poulenard, J., Giguët-Covex, C., Wilhelm, B., Révillon, S., Jenny, J.P., Revel, M., Enters, D., Bajard, M.,

Fouinat, L., Doyen, E., Simonneau, A., Pignol, C., Chapron, E. and Sabatier, P. (2016) Erosion under climate and human pressures: An alpine lake sediment perspective. *Quatern. Sci. Rev.*, **152**, 1–18.

Arnaud, F., Révillon, S., Debret, M., Revel, M., Chapron, E., Jacob, J., Giguët-Covex, C., Poulenard, J. and Magny, M. (2012) Lake Bourget regional erosion patterns reconstruction reveals Holocene NW European Alps soil evolution and paleohydrology. *Quatern. Sci. Rev.*, **51**, 81–92.

Atwater, B.F., Tuttle, M.P., Schweig, E.S., Rubin, C.M., Yamaguchi, D.K. and Hemphill-Haley, E. (2003) Earthquake recurrence inferred from paleoseismology. *Develop. Quatern. Sci.*, **1**, 331–350.

Baize, S., Cushing, M., Lemeille, F., Gelis, C., Texier, D., Nicoud, G. and Schwenninger, J.L. (2011) Contribution to the seismic hazard assessment of a slow active fault, the Vuache fault in the southern Molasse basin (France). *Bull. Soc. Géol. France*, **182**, 347–365.

Baize, S., Cushing, E.M., Lemeille, F. and Jomard, H. (2013) Updated seismotectonic zoning scheme of Metropolitan France, with reference to geologic and seismotectonic data. *Bulletin de la Société Géologique de France*, **184**(3), 225–259.

Bajard, M., Sabatier, P., David, F., Develle, A.-L., Reyss, J.-L., Fanget, B., Malet, E., Arnaud, D., Augustin, L., Crouzet, C., Poulenard, J. and Arnaud, F. (2016) Erosion record in Lake La Thuile sediments (Prealps, France): evidence of montane landscape dynamics throughout the Holocene. *Holocene*, **26**, 350–364.

Beck, C. (2009) Late Quaternary lacustrine paleo-seismic archives in north-western Alps: examples of earthquake-origin assessment of sedimentary disturbances. *Earth-Sci. Rev.*, **96**, 327–344.

Beck, C., Manalt, F., Chapron, E., Van Rensbergen, P. and De Batist, M. (1996) Enhanced seismicity in the early post-glacial period: evidence from the post-Würm sediments of Lake Annecy, northwestern Alps. *J. Geodyn.*, **22**(1–2), 155–171.

Beck, C., Van Rensbergen, P., De Batist, M., Berthier, F., Lallier, S. and Manalt, F. (2001) The Late Quaternary sedimentary infill of Lake Annecy (northwestern Alps): an overview from two seismic-reflection surveys. *J. Paleolimnol.*, **25**(2), 149–161.

Beck, C., Mercier de Lépinay, B., Schneider, J.-L., Cremer, M., Çağatay, N., Wendenbaum, E., Boutareaud, S., Ménot, G., Schmidt, S., Weber, O., Eris, K., Armijo, R., Meyer, B., Pondard, N., Gutscher, M.-A., Turon, J.-L., Labeyrie, L., Cortijo, E., Gallet, Y., Bouquerel, H., Gorur, N., Gervais, A., Castera, M.-H., Londeix, L., de Rességuier, A. and Jaouen, A. (2007) Late Quaternary co-seismic sedimentation in the Sea of Marmara's deep basins. *Sed. Geol.*, **199**(1–2), 65–89.

Becker, A., Ferry, M., Monecke, K., Schnellmann, M. and Giardini, D. (2005) Multiarchive paleoseismic record of late Pleistocene and Holocene strong earthquakes in Switzerland. *Tectonophysics*, **400**, 153–177.

Bellier, O., Cushing, E.M. and Sébrier, M. (2021) Thirty years of paleoseismic research in metropolitan France. *Comptes Rendus. Géosci.*, **353**, 339–380.

Bellwald, B. (2012) Paleoseismologic Implications of the Sediment Stratigraphy in Lake Silvaplana (Engadine, Eastern Switzerland). Doctoral dissertation, ETH.

Billiet, A. (1851) Mémoire sur les tremblements de terre ressentis en Savoie. *Mém. Acad. R. Sav.*, 1(Série 2), 244–282.

- Blaauw, M.** (2010) Methods and code for 'classical' age-modelling of radiocarbon sequences. *Quatern. Geochronol.*, **5**(5), 512–518.
- Blasio, F.V.D., Dattola, G. and Crosta, G.B.** (2018) Extremely energetic rockfalls. *J. Geophys. Res. Earth*, **123**(10), 2392–2421.
- Bodin, X., Schoeneich, P., Deline, P., Ravel, L., Magnin, F., Krysiecki, J.M. and Echelard, T.** (2015) Mountain permafrost and associated geomorphological processes: recent changes in the French Alps. *J. Alpine Res.*, 103–102. <https://doi.org/10.4000/rga.2885>
- Brooks, G.R.** (2018) Deglacial record of palaeoearthquakes interpreted from mass transport deposits at three lakes near Rouyn-Noranda, north-western Quebec, Canada. *Sedimentology*, **65**(7), 2439–2467.
- Brooks, G.R.** (2020) Evidence of a strong paleoearthquake in ~9.1 ka cal BP interpreted from mass transport deposits, western Quebec–northeastern Ontario, Canada. *Quatern. Sci. Rev.*, **234**, 106250.
- Bungum, H., Olesen, O., Pascal, C., Gibbons, S., Lindholm, C. and Vestøl, O.** (2010) To what extent is the present seismicity of Norway driven by post-glacial rebound? *J. Geol. Soc. London*, **167**(2), 373–384.
- Burkhard, M. and Sommaruga, A.** (1998) Evolution of the western Swiss Molasse basin: structural relations with the Alps and the Jura belt. *Geol. Soc. Lond. Spec. Publ.*, **134**, 279–298.
- Calais, E., Camelbeeck, T., Stein, S., Liu, M. and Craig, T.J.** (2016) A new paradigm for large earthquakes in stable continental plate interiors. *Geophys. Res. Lett.*, **43**(20), 10–621.
- Campos, C., Beck, C., Crouzet, C., Demory, F., Van Welden, A. and Eris, K.** (2013) Deciphering hemipelagites from homogenites through anisotropy of magnetic susceptibility. Paleoseismic implications (Sea of Marmara and Gulf of Corinth). *Sediment. Geol.*, **292**, 1–14.
- Cara, M., Cansi, Y., Schlupp, A., Arroucau, P., Béthoux, N., Beucler, E., Bruno, S., Calvet, M., Chevrot, S., Deboissy, A., Delouis, B., Deniel, M., Deschamps, A., Doubre, C., Fréchet, J., Godey, S., Golle, O., Grunberg, M., Guilbert, J., Haugmard, M., Jenatton, L., Lambotte, S., Leobal, D., Maron, C., Mendel, V., Merrer, S., Macquet, M., Mignan, A., Mocquet, A., Nicolas, M., Perrot, J., Potin, B., Sanchez, O., Sautoire, J.-P., Sèbe, O., Sylvander, M., Thouvenot, F., Woerd, J.V.D. and Woerd, K.V.D.** (2015) SI-Hex: a new catalogue of instrumental seismicity for metropolitan France. *Bulletin de la Société Géologique de France*, **186**(1), 3–19.
- Chapron, E., Beck, C., Pourchet, M. and Deconinck, J.-F.** (1999) 1822 earthquake-triggered homogenite in Lake Le Bourget (NW Alps). *Terra Nova*, **11**(2–3), 86–92.
- Chapron, E., Simonneau, A., Ledoux, G., Arnaud, F., Lajeunesse, P. and Albéric, P.** (2016) French Alpine Foreland Holocene paleoseismicity revealed by coeval mass wasting deposits in glacial lakes. In: *Submarine Mass Movements and their Consequences*, pp. 341–349. Springer, Cham.
- Chapron, E., Van Rensbergen, P., Beck, C., De Batist, M. and Paillet, A.** (1996) Lacustrine sedimentary records of brutal events in Lake Le Bourget (Northwestern Alps–Southern Jura). *Quaternaire*, **7**(2), 155–168.
- Chiarle, M., Geertsema, M., Mortara, G. and Clague, J.J.** (2021) Relations between climate change and mass movement: perspectives from the Canadian Cordillera and the European Alps. *Global Planet. Change*, **202**, 103499.
- Cita, M.B. and Rimoldi, B.** (1997) Geological and geophysical evidence for a holocene tsunami deposit in the astern Mediterranean deep-sea record. *J. Geodyn.*, **24** (1–4), 293–304.
- Clark, C.D., Hughes, A.L.C., Greenwood, S.L., Jordan, C. and Sejrup, H.P.** (2010) Pattern and timing of retreat of the last British–Irish Ice Sheet. *Quatern Sci. Rev.*, **44**, 112–146.
- Cossart, E., Braucher, R., Fort, M., Bourlès, D.L. and Carcaillet, J.** (2008) Slope instability in relation to glacial debuitressing in alpine areas (Upper Durance catchment, southeastern France): Evidence from field data and ¹⁰Be cosmic ray exposure ages. *Geomorphol. Paraglac. Geomorphol. Proc. Paraglac. Cont.*, **95**(1–2), 3–26.
- Coutterand, S.** (2010) Etude géomorphologique des flux glaciaires dans les Alpes nord-occidentales au Pléistocène récent: du maximum de la dernière glaciation aux premières étapes de la déglaciation. Doctoral dissertation, Chambéry.
- Crouzet, C., Wilhelm, B., Sabatier, P., Demory, F., Thouveny, N., Pignol, C., Reyss, J.-L., Magand, O., Jeltsch-Thömmes, A., Bajard, M., Augustin, L. and Arnaud, F.** (2019) Palaeomagnetism for chronologies of recent alpine lake sediments: successes and limits. *J. Paleolimnol.*, **62**, 259–278.
- Delaney, I. and Adhikari, S.** (2020) Increased subglacial sediment discharge in a warming climate: Consideration of ice dynamics, glacial erosion, and fluvial sediment transport. *Geophys. Res. Lett.*, **47**(7). <https://doi.org/10.1029/2019GL085672>
- Deline, P., Gruber, S., Amann, F., Bodin, X., Delaloye, R., Failletaz, J., Fischer, L., Geertsema, M., Giardino, M., Hasler, A., Kirkbride, M., Krautblatter, M., Magnin, F., McColl, S., Ravel, L., Schoeneich, P. and Weber, S.** (2021) Ice loss from glaciers and permafrost and related slope instability in high-mountain regions. In: *Snow and Ice-Related Hazards, Risks, and Disasters*, pp. 501–540. Elsevier. <https://doi.org/10.1016/B978-0-12-817129-5.00015-9>
- Delmas, M., Calvet, M. and Gunnell, Y.** (2009) Variability of Quaternary glacial erosion rates: a global perspective with special reference to the Eastern Pyrenees. *Quatern. Sci. Rev.*, **28**(5–6), 484–498.
- Demory, F., Uehara, M., Quesnel, Y., Rochette, P., Romey, C., Tachikawa, K., Garcia, M., Borscheck, D., Pignol, L., Bard, E. and Andrieu-Ponel, V.** (2019) A new high-resolution magnetic scanner for sedimentary sections. *Geochem. Geophys. Geosyst.*, **20**(7), 3186–3200.
- Deparis, J., Jongmans, D., Cotton, F., Baillet, L., Thouvenot, F. and Hantz, D.** (2008) Analysis of rock-fall and rock-fall avalanche seismograms in the French Alps. *Bull. Seismol. Soc. Am.*, **98**(4), 1781–1796.
- Drouet, S., Ameri, G., Le Dortz, K., Secanell, R. and Senfaute, G.** (2020) A probabilistic seismic hazard map for the metropolitan France. *Bull. Earthquake Eng.*, **18**(5), 1865–1898.
- Eriş, K.K., Çağatay, N., Beck, C., Mercier de Lepinay, B. and Corina, C.** (2012) Late-Pleistocene to Holocene sedimentary fills of the Çınarcık Basin of the Sea of Marmara. *Sed. Geol.*, **281**, 151–165.
- Forsberg, C.F., Heyerdahl, H. and Solheim, A.** (2016) Underwater mass movements in Lake Mjøsa, Norway. *Advances in Natural and Technological Hazards Research*, 191–199.
- Forwick, M. and Vorren, T.O.** (2002) Deglaciation history and post-glacial mass movements in Balsfjord, northern Norway. *Polar Res.*, **21**(2), 259–266.

- Gastineau, R., De Sigoyer, J., Sabatier, P., Fabbri, S.C., Anselmetti, F.S., Develle, A.L., Şahin, M., Gündüz, S., Niessen, F. and Gebhardt, A.C. (2021) Active subaquatic fault segments in Lake Iznik along the middle strand of the North Anatolian Fault, NW Turkey. *Tectonics*, **40**(1), e2020TC006404.
- Gatter, R., Clare, M.A., Kuhlmann, J. and Huhn, K. (2021) Characterisation of weak layers, physical controls on their global distribution and their role in submarine landslide formation. *Earth Sci. Rev.*, **223**, 103845.
- Geertsema, M. and Foord, V.N. (2014) Landslides in the isolated patches permafrost zone, northeastern British Columbia (NTS mapsheet 94G east half). In: *Landslide Science for a Safer Geoenvironment*, pp. 451–455. Springer, Cham.
- de Gelder, G., Doan, M.L., Beck, C., Carlut, J., Seibert, C., Feuillet, N., Carter, G.D.O., Pechlivanidou, S. and Gawthorpe, R.L. (2022) Multi-scale and multi-parametric analysis of Late Quaternary event deposits within the active Corinth Rift (Greece). *Sedimentology*, **69**(4), 1573–1598.
- Gidon, P. (1962) *Carte géologique détaillée de la France à 1/50.000, feuille Chambéry*. BRGM Edition, Orléans.
- Gidon, M. and Barféty, J.C. (1969) *Carte géologique détaillée de la France à 1/50.000, feuille Montmélian*. BRGM Edition, Orléans.
- Gruber, S., Hoelzle, M. and Haeberli, W. (2004) Permafrost thaw and destabilization of Alpine rock walls in the hot summer of 2003. *Geophys. Res. Lett.*, **31**(13), 1–4.
- Hasegawa, H.S. and Basham, P.W. (1989) Spatial correlation between seismicity and postglacial rebound in eastern Canada. In: *Earthquakes at North-Atlantic Passive Margins: Neotectonics and Postglacial Rebound*, pp. 483–500. Springer, Dordrecht.
- Heiri, O., Lotter, A.F. and Lemcke, G. (2001) Loss on ignition as a method for estimating organic and carbonate content in sediments: reproducibility and comparability of results. *J. Paleolimnol.*, **25**(1), 101–110.
- Hilbe, M. and Anselmetti, F.S. (2014) Signatures of slope failures and river-delta collapses in a perialpine lake (Lake Lucerne, Switzerland). *Sedimentology*, **61**, 1883–1907.
- Hoek, W.Z. (2008) The last glacial-interglacial transition. *Episodes*, **31**(2), 226–229.
- Huggel, C. (2009) Recent extreme slope failures in glacial environments: effects of thermal perturbation. *Quatern. Sci. Rev.*, **28**(11–12), 1119–1130.
- Jakobsson, M., Björck, S., O'Regan, M., Flodén, T., Greenwood, S.L., Swärd, H., Lif, A., Ampel, L., Koyi, H. and Skelton, A. (2014) Major earthquake at the Pleistocene-Holocene transition in Lake Vättern, southern Sweden. *Geology*, **42**(5), 379–382.
- Jargot, M. and Loup, J. (1983) Un cas particulier de pollution lacustre: le lac d'Aiguebelette. *Revue de géographie alpine*, **71**(4), 399–405.
- Jelinek, V. (1981) Characterization of the magnetic fabric of rocks. *Tectonophysics*, **79**(3–4), T63–T67.
- Jenner, K.A., Piper, D.J., Campbell, D.C. and Mosher, D.C. (2007) Lithofacies and origin of late Quaternary mass transport deposits in submarine canyons, central Scotian Slope, Canada. *Sedimentology*, **54**(1), 19–38.
- Jomard, H., Cushing, E.M., Palumbo, L., Baize, S., David, C. and Chartier, T. (2017) Transposing an active fault database into a seismic hazard fault model for nuclear facilities – part 1: building a database of potentially active faults (BDFa) for metropolitan France. *Nat. Hazards Earth Syst. Sci.*, **17**(9), 1573–1584.
- Jomard, H., Scotti, O., Auclair, S., Dominique, P., Manchuel, K. and Sicilia, D. (2021) The SISFRANCE database of historical seismicity. State of the art and perspectives. *Comptes Rendus. Géosci.*, **353**(S1), 1–24.
- Kastens, K.A. and Cita, M.B. (1981) Tsunami-induced sediment transport in the abyssal Mediterranean Sea. *Geol. Soc. Am. Bull.*, **92**(11), 845–857.
- Kremer, K., Gassner-Stamm, G., Grolimund, R., Wirth, S.B., Strasser, M. and Fäh, D. (2020) A database of potential paleoseismic evidence in Switzerland. *J. Seismol.*, **24**(2), 247–262.
- Kremer, K., Hilbe, M., Simpson, G., Decrouy, L., Wildi, W. and Girardclos, S. (2015) Reconstructing 4000 years of mass movement and tsunami history in a deep peri-Alpine lake (Lake Geneva, France-Switzerland). *Sedimentology*, **62**(5), 1305–1327.
- Kremer, K., Simpson, G. and Girardclos, S. (2012) Giant Lake Geneva tsunami in AD 563. *Nat. Geosci.*, **5**(11), 756–757.
- Kremer, K., Wirth, S.B., Reusch, A., Fäh, D., Bellwald, B., Anselmetti, F.S., Girardclos, S. and Strasser, M. (2017) Lake-sediment based paleoseismology: Limitations and perspectives from the Swiss Alps. *Quatern. Sci. Rev.*, **168**, 1–18.
- de La Taille, C., Jouanne, F., Crouzet, C., Beck, C., Jomard, H., De Rycker, K. and Van Daele, M. (2015) Impact of active faulting on the post LGM infill of Le Bourget Lake (western Alps, France). *Tectonophysics*, **664**, 31–49.
- Larroque, C., Baize, S., Albaric, J., Jomard, H., Trévisan, J., Godano, M., Cushing, M., Deschamps, A., Sue, C., Delouis, B., Potin, B., Courboux, F., Régnier, M., Rivet, D., Chêze, J., Martin, X., Maron, C. and Peix, F. (2021) Seismotectonics of southeast France: from the Jura mountains to Corsica. *Comptes Rendus. Géoscience*, **353**(S1), 105–151.
- Lefebvre, P., Gourgiotis, A., Mangeret, A., Sabatier, P., Le Pape, P., Diez, O., Louvat, P., Menguy, N., Merrot, P., Baya, C., Zebracki, M., Blanchart, P., Malet, E., Jézéquel, D., Reyss, J.-L., Bargar, J.R., Gaillardet, J., Cazala, C. and Morin, G. (2021) Diagenetic formation of uranium-silica polymers in lake sediments over 3,300 years. *Proc. Natl Acad. Sci. USA*, **118**, e2021844118.
- Lin, C.H., Jan, J.C., Pu, H.C., Tu, Y., Chen, C.C. and Wu, Y.M. (2015) Landslide seismic magnitude. *Earth Planet. Sci. Lett.*, **429**, 122–127.
- Locat, J., Leroueil, S., Locat, A. and Lee, H. (2014) Weak layers: their definition and classification from a geotechnical perspective. In: *Submarine Mass Movements and their Consequences*, pp. 3–12. Springer, Cham.
- Lowag, J., Bull, J.M., Vardy, M.E., Miller, H. and Pinson, L.J.W. (2012) High-resolution seismic imaging of a Younger Dryas and Holocene mass movement complex in glacial lake Windermere, UK. *Geomorphology*, **171**, 42–57.
- Magny, M., Aalbersberg, G., Bégeot, C., Benoit-Ruffaldi, P., Bossuet, G., Disnar, J.-R., Heiri, O., Laggoun-Defarge, F., Mazier, F., Millet, L., Peyron, O., Vannière, B. and Walter-Simonnet, A.-V. (2006) Environmental and climatic changes in the Jura mountains (Eastern France) during the Lateglacial–Holocene transition: a multi-proxy record from Lake Lautrey. *Quatern. Sci. Rev.*, **25**(5–6), 414–445.
- Manchuel, K., Traversa, P., Baumont, D., Cara, M., Nayman, E. and Durouchoux, C. (2018) The French seismic CATalogue (FCAT-17). *Bull. Earthquake Eng.*, **16**, 2227–2251.

- Manconi, A., Picozzi, M., Coviello, V., De Santis, F. and Elia, L. (2016) Real-time detection, location, and characterization of rockslides using broadband regional seismic networks. *Geophys. Res. Lett.*, **43**(13), 6960–6967.
- Mazzotti, S., Jomard, H. and Masson, F. (2020) Processes and deformation rates generating seismicity in metropolitan France and conterminous Western Europe. *BSGF-Earth Sci. Bull.*, **191**(1), 19.
- McCalpin, J.P. (2009) Application of Paleoseismic Data to Seismic Hazard Assessment and Neotectonic Research. *Intern. Geophys. Paleoseismol.*, **95**, 1–106.
- McHugh, C.M., Seeber, L., Braudy, N., Cormier, M.-H., Davis, M.B., Diebold, J.B., Dieudonne, N., Douilly, R., Gulick, S.P.S., Hornbach, M.J., Johnson, H.E., Mishkin, K.R., Sorlien, C.C., Steckler, M.S., Symithe, S.J. and Templeton, J. (2011) Offshore sedimentary effects of the 12 January 2010 Haiti earthquake. *Geology*, **39**(8), 723–726.
- Moernaut, J. and De Batist, M. (2011) Frontal emplacement and mobility of sublacustrine landslides: results from morphometric and seismostratigraphic analysis. *Mar. Geol.*, **285**(1–4), 29–45.
- Moernaut, J., Van Daele, M., Fontijn, K., Heirman, K., Kempf, P., Pino, M., Valdebenito, G., Urrutia, R., Strasser, M. and De Batist, M. (2018) Larger earthquakes recur more periodically: New insights in the megathrust earthquake cycle from lacustrine turbidite records in south-central Chile. *Earth Planet. Sci. Lett.*, **481**, 9–19.
- Monecke, K., Anselmetti, F.S., Becker, A., Schnellmann, M., Sturm, M. and Giardini, D. (2006) Earthquake-induced deformation structures in lake deposits: a Late Pleistocene to Holocene paleoseismic record for Central Switzerland. *Eclogae Geologicae Helvetiae*, **99**(3), 343–362.
- Mörner, N.A. (2004) Active faults and paleoseismicity in Fennoscandia, especially Sweden. Primary structures and secondary effects. *Tectonophy. Active Fault Eastern Hemis.*, **380**(3–4), 139–157.
- Mulder, T. and Alexander, J. (2001) The physical character of subaqueous sedimentary density flows and their deposits. *Sedimentology*, **48**(2), 269–299.
- Mulder, T. and Cochonat, P. (1996) Classification of offshore mass movements. *J. Sediment. Res.*, **66**(1), 43–57.
- Mutti, E., Bernoulli, D., Lucchi, F.R. and Tinterri, R. (2009) Turbidites and turbidity currents from Alpine ‘flysch’ to the exploration of continental margins. *Sedimentology*, **56**(1), 267–318.
- Nicoud, G., Dzikowski, M., Paillet, A., Ghoreychi, R., Emeric, P. and Chignoli, M. (1999) Données nouvelles sur la nature et l’extension du glissement historique du Granier (Savoie, France). In *Mémoire de l’académie de Savoie (actes du colloque de Myans)*, pp. 35–54.
- Nikolaeva, S.B., Nikonov, A.A., Shvarev, S.V. and Rodkin, M.V. (2016) Comprehensive paleoseismic geological studies in a key site in southwestern Kola Peninsula (Northeast of the Fennoscandian Shield). *Doklady Earth Sci.*, **469**(1), 656–660.
- Noetzli, J., Hoelzle, M. and Haeblerli, W. (2003, July) Mountain permafrost and recent Alpine rock-fall events: a GIS-based approach to determine critical factors. In: *Proceedings of the 8th International Conference on Permafrost* (Vol. 2, pp. 827–832). Swets & Zeitlinger Lisse, Zürich.
- Nomade, J. (2005) Chronologie et sédimentologie du remplissage du lac d’Annecy depuis le Tardiglaciaire: Implications paléoclimatologiques et paléohydrologiques. Doctoral dissertation, Université Joseph-Fourier-Grenoble I. PhD thesis.
- Nygard, A., Sejrup, H.P., Haflidason, H., Lekens, W.A.H., Clark, C.D. and Bigg, G.R. (2007) Extreme sediment and ice discharge from marine-based ice streams: new evidence from the North Sea. *Geology*, **35**(5), 395–398.
- Ojala, A.E., Mattila, J., Hämäläinen, J. and Sutinen, R. (2019) Lake sediment evidence of paleoseismicity: timing and spatial occurrence of late-and postglacial earthquakes in Finland. *Tectonophysics*, **771**, 228227.
- Oswald, P., Moernaut, J., Fabbri, S.C., De Batist, M., Hajdas, I., Ortner, H., Titzler, S. and Strasser, M. (2021) Combined on-fault and off-fault paleoseismic evidence in the postglacial infill of the inner-alpine lake Achensee (Austria, Eastern Alps). *Front. Earth Sci.*, **9**, 438.
- Oswald, P., Strasser, M., Skapski, J. and Moernaut, J. (2022) Magnitude and source area estimations of severe prehistoric earthquakes in the western Austrian Alps. *Nat. Hazards Earth Syst. Sci.*, **22**(6), 2057–2079.
- Pachoud, A. (1991) Une catastrophe naturelle majeure : l’écroulement du Mont Granier dans le massif de la Chartreuse au XIIIe siècle. *La Houille Blanche*, **5**, 327–332.
- Peizhen, Z., Molnar, P. and Downs, W.R. (2001) Increased sedimentation rates and grain sizes 2–4 Myr ago due to the influence of climate change on erosion rates. *Nature*, **410**, 891–897.
- Pellegrini, G.B., Surian, N. and Albanese, D. (2006) Landslide activity in response to alpine deglaciation: the case of the Belluno Prealps (Italy). *Geogr. Fis. Din. Quat.*, **29**, 185–196.
- Petersen, J., Wilhelm, B., Revel, M., Rolland, Y., Crouzet, C., Arnaud, F., Brisset, E., Chaumillon, E. and Magand, O. (2014) Sediments of Lake Vens (SW European Alps, France) record large-magnitude earthquake events. *J. Paleolimnol.*, **51**(3), 343–355.
- Pirulli, M. (2009) The Thurwieser rock avalanche (Italian Alps): Description and dynamic analysis. *Eng. Geol.*, **109**(1–2), 80–92.
- Praet, N., Moernaut, J., Van Daele, M., Boes, E., Haeussler, P.J., Strupler, M., Schmidt, S., Loso, M. and De Batist, M. (2017) Paleoseismic potential of sublacustrine landslide records in a high-seismicity setting (south-central Alaska). *Mar. Geol.*, **384**, 103–119.
- Prior, D.B., Coleman, J.M. and Bornhold, B.D. (1982) Results of a known seafloor instability event. *Geo-Mar. Lett.*, **2**(3), 117–122.
- R Core Team (2020) *R: A Language and Environment for Statistical Computing*. R Foundation for Statistical Computing, Vienna, Austria.
- Rabin, M., Sue, C., Walpersdorf, A., Sakic, P., Albaric, J. and Fores, B. (2018) Present-day deformations of the Jura arc inferred by GPS surveying and earthquake focal mechanisms. *Tectonics*, **37**, 3782–3804.
- Rapuc, W., Sabatier, P., Andrič, M., Crouzet, C., Arnaud, F., Chapron, E., Šmuc, A., Develle, A., Wilhelm, B., Demory, F., Reyss, J., Régnier, E., Daut, G. and Von Grafenstein, U. (2018) 6600 years of earthquake record in the Julian Alps (Lake Bohinj, Slovenia). *Sedimentology*, **65**(5), 1777–1799.
- Reimer, P.J., Austin, W.E.N., Bard, E., Bayliss, A., Blackwell, P.G., Ramsey, C.B., Butzin, M., Cheng, H., Edwards, R.L., Friedrich, M., Grootes, P.M., Guilderson, T.P., Hajdas, I., Heaton, T.J., Hogg, A.G., Hughen, K.A., Kromer, B., Manning, S.W., Muscheler, R., Palmer, J.G., Pearson, C., van der Plicht, J., Reimer, R.W., Richards, D.A., Scott, E.M., Southon, J.R., Turney, C.S.M., Wacker, L., Adolphi, F., Büntgen, U., Capano, M., Fahrni, S.M., Fogtmann-Schulz, A., Friedrich, R., Köhler, P., Kudsk, S.,

- Miyake, F., Olsen, J., Reinig, F., Sakamoto, M., Sookdeo, A. and Talamo, S. (2020) The IntCal20 northern hemisphere radiocarbon age calibration curve (0–55 cal kBP). *Radiocarbon*, **62**, 725–757.
- Roattino, T., Crouzet, C., Vassallo, R., Buoncristiani, J.F., Carcaillet, J., Gribenski, N. and Valla, P.G. (2022) Paleogeographical reconstruction of the western French Alps foreland during the last glacial maximum using cosmogenic exposure dating. *Quatern. Res.*, 1–16. <https://doi.org/10.1017/qua.2022.25>
- Sabatier, P., Wilhelm, B., Ficetola, G.F., Moiroux, F., Poulenard, J., Develle, A.L., Bichet, A., Chen, W., Pignol, C., Reyss, J.-L., Gielly, L., Bajard, M., Perrette, Y., Malet, E., Taberlet, P. and Arnaud, F. (2017) 6-kyr record of flood frequency and intensity in the western Mediterranean Alps—Interplay of solar and temperature forcing. *Quatern. Sci. Rev.*, **170**, 121–135.
- Sammartini, M., Moernaut, J., Anselmetti, F.S., Hilbe, M., Lindhorst, K., Praet, N. and Strasser, M. (2019) An atlas of mass-transport deposits in lakes. In: *Submarine Landslides: Subaqueous Mass Transport Deposits from Outcrops to Seismic Profiles* (Eds Ogata, K., Festa, A., Pini, G. A.), *Geophys. Monogr. Ser.*, 201–226.
- Sammartini, M., Moernaut, J., Kopf, A., Stegmann, S., Fabbri, S.C., Anselmetti, F.S. and Strasser, M. (2021) Propagation of frontally confined subaqueous landslides: insights from combining geophysical, sedimentological, and geotechnical analysis. *Sediment. Geol.*, **416**, 105877.
- Sánchez, L., Völksen, C., Sokolov, A., Arenz, H. and Seitz, F. (2018) Present-day surface deformation of the Alpine region inferred from geodetic techniques. *Earth Syst. Sci. Data*, **10**, 1503–1526.
- Schnellmann, M.P. (2004) Late quaternary mass-movements in a perialpine lake (Lake Lucerne, Switzerland): sedimentary processes, natural hazards and paleoseismic reconstructions. Doctoral dissertation, ETH Zurich. PhD thesis.
- Schnellmann, M., Anselmetti, F.S., Giardini, D. and McKenzie, J.A. (2005) Mass movement-induced fold-and-thrust belt structures in unconsolidated sediments in Lake Lucerne (Switzerland). *Sedimentology*, **52**(2), 271–289.
- Shanmugam, G. (2002) Ten turbidite myths. *Earth-Sci. Rev.*, **58**(3–4), 311–341.
- Shipp, R.C., Weimer, P. and Posamentier, H.W. (Eds) (2011) *Mass-Transport Deposits in Deepwater Settings*. SEPM Special Publication.
- Sommaruga, A. (1999) Décollement tectonics in the Jura foreland fold-and-thrust belt. *Marine Petrol. Geol.*, **16**(2), 111–134.
- Stein, S. and Mazzotti, S. (Eds) (2007) Continental intraplate earthquakes: science, hazard, and policy issues (Vol. 425). Geological Society of America. <https://doi.org/10.1130/SPE425>
- Sternai, P., Sue, C., Husson, L., Serpelloni, E., Becker, T.W., Willett, S.D., Faccenna, C., Di Giulio, A., Spada, G., Jolivet, L., Valla, P., Petit, C., Nocquet, J.M., Walpersdorf, A. and Castelltort, S. (2019) Present-day uplift of the European Alps: Evaluating mechanisms and models of their relative contributions. *Earth-Sci. Rev.*, **190**, 589–604.
- Stewart, I.S., Sauber, J. and Rose, J. (2000) Glacio-seismotectonics: ice sheets, crustal deformation and seismicity. *Quatern. Sci. Rev.*, **19**(14–15), 1367–1389.
- Strasser, M. (2008) *Quantifying Late Quaternary Natural Hazards in Swiss Lakes: Subaquatic Landslides, Slope Stability Assessments, Paleoseismic Reconstructions and Lake Outbursts*, Vol. 95. ETH Zurich. <https://www.research-collection.ethz.ch/bitstream/handle/20.500.11850/150306/1/eth-30202-01.pdf>
- Strasser, M., Anselmetti, F.S., Fäh, D., Giardini, D. and Schnellmann, M. (2006) Magnitudes and source areas of large prehistoric northern Alpine earthquakes revealed by slope failures in lakes. *Geology*, **34**(12), 1005–1008.
- Strasser, M., Monecke, K., Schnellmann, M. and Anselmetti, F.S. (2013) Lake sediments as natural seismographs: a compiled record of Late Quaternary earthquakes in Central Switzerland and its implication for Alpine deformation. *Sedimentology*, **60**, 319–341.
- Talling, P.J., Masson, D.G., Sumner, E.J. and Malgesini, G. (2012) Subaqueous sediment density flows: depositional processes and deposit types. *Sedimentology*, **59**(7), 1937–2003.
- Tanty, C., Valet, J.P., Carlut, J., Bassinot, F. and Zaragosi, S. (2016) Acquisition of detrital magnetization in four turbidites. *Geochem. Geophys. Geosyst.*, **17**(8), 3207–3223.
- Turpeinen, H., Hampel, A., Karow, T. and Maniatis, G. (2008) Effect of ice sheet growth and melting on the slip evolution of thrust faults. *Earth Planet. Sci. Lett.*, **269**(1–2), 230–241.
- Van Daele, M., Moernaut, J., Doom, L., Boes, E., Fontijn, K., Heirman, K., Vandroone, W., Hebbeln, D., Pino, M., Urrutia, R., Brümmer, R. and De Batist, M. (2015) A comparison of the sedimentary records of the 1960 and 2010 great Chilean earthquakes in 17 lakes: Implications for quantitative lacustrine palaeoseismology. *Sedimentology*, **62**(5), 1466–1496.
- Van Rensbergen, P., De Batist, M., Beck, C. and Chapron, E. (1999) High-resolution seismic stratigraphy of glacial to interglacial fill of a deep glacial lake: Lake Le Bourget, Northwestern Alps, France. *Sediment. Geol.*, **128**(1–2), 99–129.
- Van Rensbergen, P., De Batist, M., Beck, C. and Manalt, F. (1998) High resolution seismic stratigraphy of late Quaternary fill of Lake Annecy (Northwestern Alps): evolution from glacial to interglacial sedimentary processes. *Sediment. Geol.*, **117**(1–2), 61–86.
- Vardy, M.E., Pinson, L.J.W., Bull, J.M., Dix, J.K., Henstock, T.J., Davis, J.W. and Gutowski, M. (2010) 3D seismic imaging of buried Younger Dryas mass movement flows: Lake Windermere, UK. *Geomorphology*, **118**, 176–187.
- Wells, D.L. and Coppersmith, K.J. (1994) New empirical relationships among magnitude, rupture length, rupture width, rupture area, and surface displacement. *Bull. Seismol. Soc. Am.*, **84**(4), 974–1002.
- Weltje, G.J., Bloemsma, M.R., Tjallingii, R., Heslop, D., Röhl, U. and Croudace, I.W. (2015) Chapter 21: Prediction of geochemical composition from XRF core scanner data: a new multivariate approach including automatic selection of calibration samples and quantification of uncertainties. In: *Micro-XRF Studies of Sediment Cores*, pp. 507–534. Springer. https://doi.org/10.1007/978-94-017-9849-5_21
- Wilhelm, B., Nomade, J., Crouzet, C., Litty, C., Sabatier, P., Belle, S., Rolland, Y., Revel, M., Courboux, F., Arnaud, F. and Anselmetti, F.S. (2016) Quantified sensitivity of small lake sediments to record historic earthquakes: implications for paleoseismology: Lake sensitivity to record earthquakes. *J. Geophys. Res. Earth Surf.*, **121**(1), 2–16.
- Wirsig, C., Zasadni, J., Christl, M., Akçar, N. and Ivy-Ochs, S. (2016) Dating the onset of LGM ice surface lowering in the High Alps. *Quatern. Sci. Rev.*, **143**, 37–50.
- Zavala, C. and Arcuri, M. (2016) Intra-basinal and extrabasinal turbidites: Origin and distinctive characteristics. *Sediment. Geol.*, **337**, 36–54.

Manuscript received 8 March 2022; revision accepted 27 September 2022

Supporting Information

Additional information may be found in the online version of this article:

Supplementary Material 1. Interpretation of calcium and titanium geochemical proxies.

Supplementary Material 2. Estimation of the regional earthquake recurrence rate.

Supplementary Material 3. Additional figures.